The Astrophysical Journal, 846:17 (20pp), 2017 September 1 https://doi.org/10.3847/1538-4357/aa821d

The Origin of the Ultraluminous X-Ray Sources

Grzegorz Wiktorowicz[1,2], Małgorzata Sobolewska[3], Jean-Pierre Lasota[2,4,5], and Krzysztof Belczynski[1,2,4]
[1] Astronomical Observatory, Warsaw University, Al. Ujazdowskie 4, 00-478 Warsaw, Poland; gwiktoro@astrouw.edu.pl
[2] Kavli Institute for Theoretical Physics, Kohn Hall, University of California, Santa Barbara, CA 93106, USA
[3] Harvard-Smithsonian Center for Astrophysics, 60 Garden Street, Cambridge, MA 02138, USA
[4] Nicolaus Copernicus Astronomical Center, Polish Academy of Sciences, Bartycka 18, 00-716 Warsaw, Poland
[5] Institut d'Astrophysique de Paris, CNRS et Sorbonne Universités, UPMC Paris 06, UMR 7095, 98bis Bd Arago, F-75014 Paris, France
Received 2017 May 17; revised 2017 July 21; accepted 2017 July 23; published 2017 August 28

Abstract

Recently, several ultraluminous X-ray (ULX) sources were shown to host a neutron star (NS) accretor. We perform a suite of evolutionary calculations, which show that, in fact, NSs are the dominant type of ULX accretor. Although black holes (BH) dominate early epochs after the star-formation burst, NSs outweigh them after a few 100 Myr and may appear as late as a few gigayears after the end of the star-formation episode. If star formation is a prolonged and continuous event (i.e., not a relatively short burst), NS accretors dominate the ULX population at any time in the solar metallicity environment, whereas BH accretors dominate when the metallicity is sub-solar. Our results show a very clear (and testable) relation between the companion/donor evolutionary stage and the age of the system. A typical NSULX consists of a $\sim$1.3 $M_{\odot}$ NS and $\sim$1.0 $M_{\odot}$ Red Giant. A typical BH ULX consists of a $\sim$8 $M_{\odot}$ BH and $\sim$6 $M_{\odot}$ main-sequence star. Additionally, we find that the very luminous ULXs ($L_X \gtrsim 10^{41}$ erg s^{-1}) are predominantly BH systems ($\sim$9 $M_{\odot}$) with Hertzsprung-gap donors ($\sim$2 $M_{\odot}$). Nevertheless, some NSULX systems may also reach extremely high X-ray luminosities ($\gtrsim 10^{41}$ erg s^{-1}).

Key words: methods: statistical – stars: black holes – stars: neutron – X-rays: binaries

1. Introduction

Ultraluminous X-ray source (ULX; for a review, see Feng & Soria 2011) is defined by two observational properties:

1. it is a point-like (i.e., not extended) off-nuclear X-ray source with a peak emission localized in the X-ray band;
2. it emits isotropic equivalent X-ray luminosity in excess of 10^{39} erg s^{-1}, which is approximately the Eddington limit (EL) for a spherically accreting stellar-mass black hole (sMBH; $\sim$10 $M_{\odot}$).

Until recently the main problem with unveiling the nature of the ULXs stemmed from the absence of reliable measurements of the masses of the accreting compact objects. This has changed with the discovery of pulsing ultraluminous X-ray sources (PULXs), which contain neutron stars (NS). The first X-ray pulsar was discovered in M82 X-2 (Bachetti et al. 2014). Then, two other PULXs have been identified: P13 in NGC 7793 (Fürst et al. 2016; Israel et al. 2017b) and NGC5907 ULX1, (Fürst et al. 2017; Israel et al. 2017a). All of these PULXs show regular pulses with periods $\sim$1 s, characteristic of NS accretors.

These discoveries proved that some ULXs do contain stellar-mass compact objects. Moreover, it is possible that NSs may reside in a vast majority of the ULXs (NSULXs; Kluźniak & Lasota 2015; King & Lasota 2016; King et al. 2017). Existence of PULXs provides strong evidence in support of the models involving a super-Eddington accretion onto a compact star (e.g., Begelman 2002; Poutanen et al. 2007; King 2009) as an explanation of the ULXs phenomenon (e.g., Körding et al. 2002).

However, apparent super-Eddington luminosities can also be reached without breaching the EL if the radiation of an accreting compact star is beamed (e.g., King et al. 2001; Poutanen et al. 2007). Detailed accretion disk simulations appear to support the importance of beaming (e.g., Ohsuga et al. 2005; Ohsuga & Mineshige 2011; Jiang et al. 2014; Sądowski & Narayan 2015).

In this study, we perform massive simulations in order to uncover the nature of the stars forming the ULX population. Motivated by the recent observational progress, we limited our investigation to the stellar-mass compact objects with super-Eddington and/or beamed emission.

2. Simulations

The calculations were performed with the use of the `StarTrack` population synthesis code (Belczynski et al. 2002, 2008) with significant updates described in Dominik et al. (2012) and Wiktorowicz et al. (2014).

We start the evolution of each system from the zero-age main sequence (ZAMS), which we assume to happen at the same moment for both stars. The primary has an initial mass of $M_a = 6$–$150\,M_{\odot}$ drawn from a power-law distribution with index -2.7 (Kroupa & Weidner 2003). The mass of the secondary (M_b) is chosen from the 0.08 to 150 $M_{\odot}$ range to preserve a uniform mass-ratio distribution. Typical predecessors of X-ray binaries (XRB) with NS or BH accretors should reside in such a range of masses. The initial separations are uniform in logarithm ($P(a) \sim 1/a$; Abt 1983). The eccentricities' distribution is the thermal-equilibrium (Duquennoy & Mayor 1991). The binary fraction was set to 50% for stars with ZAMS mass below 10 $M_{\odot}$ and 100% for systems with more massive primaries. We are aware of the results of Sana et al. (2012) who provide other relations for initial parameter distributions, but their results were obtained for stars with masses 15–60 $M_{\odot}$ and were limited to solar metallicity. Therefore, we decided to keep the previously established distributions. For comparison between our adopted and Sana

[6] Warsaw Virgo Group.

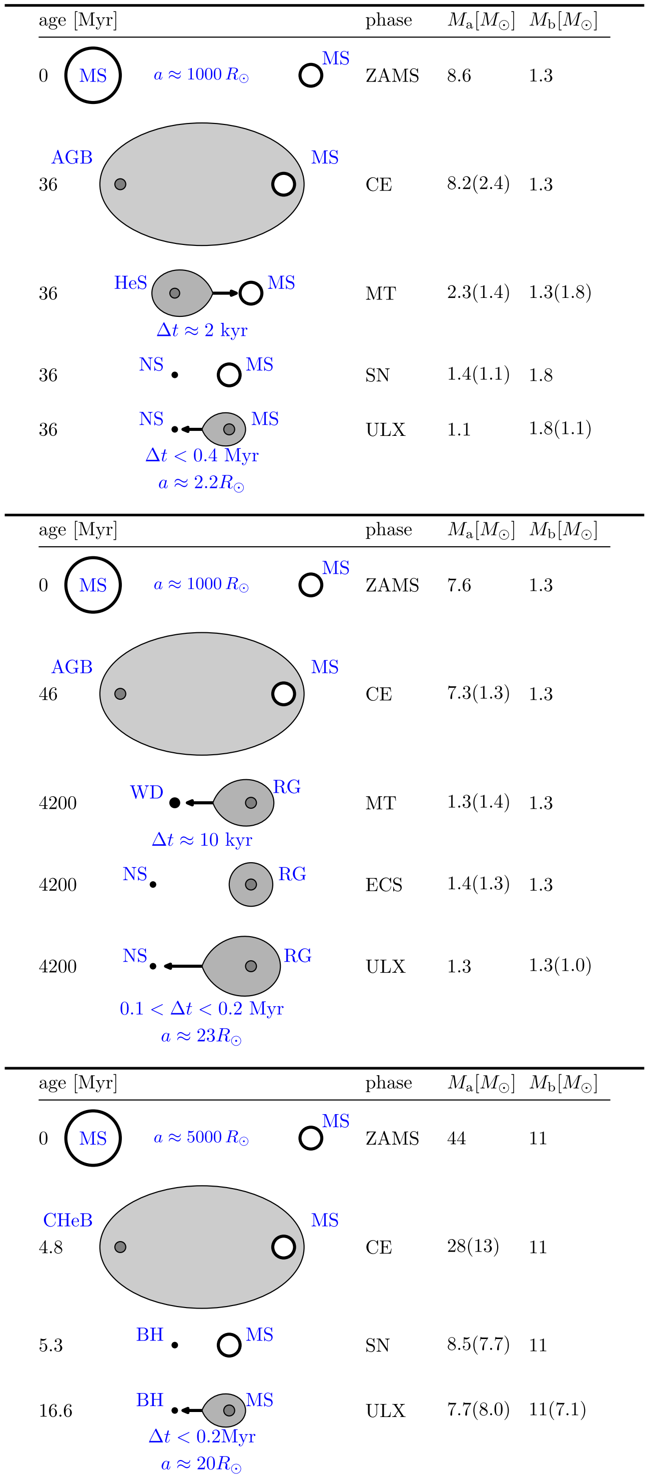

Figure 1. Schematic representation of the dominant NSULX evolutionary routes in young (top; $\mathcal{R}_{\rm NS,MS}$) and old (middle; $\mathcal{R}_{\rm NS,RG}$) stellar populations. Bottom: typical BHULX evolution (SF regions). The age and mass values reflect those in a typical system. For an explanation of abbreviations, see the text (Section 3.1). For phases in which the mass of one of the components changes rapidly, two values are provided: the mass at the beginning of a phase and at the end (in parentheses).

et al. (2012) initial distributions the reader may refer to de Mink & Belczynski (2015).

We simulated the evolution of 2×10^7 binary systems for every model and scaled the results to the Milky Way equivalent

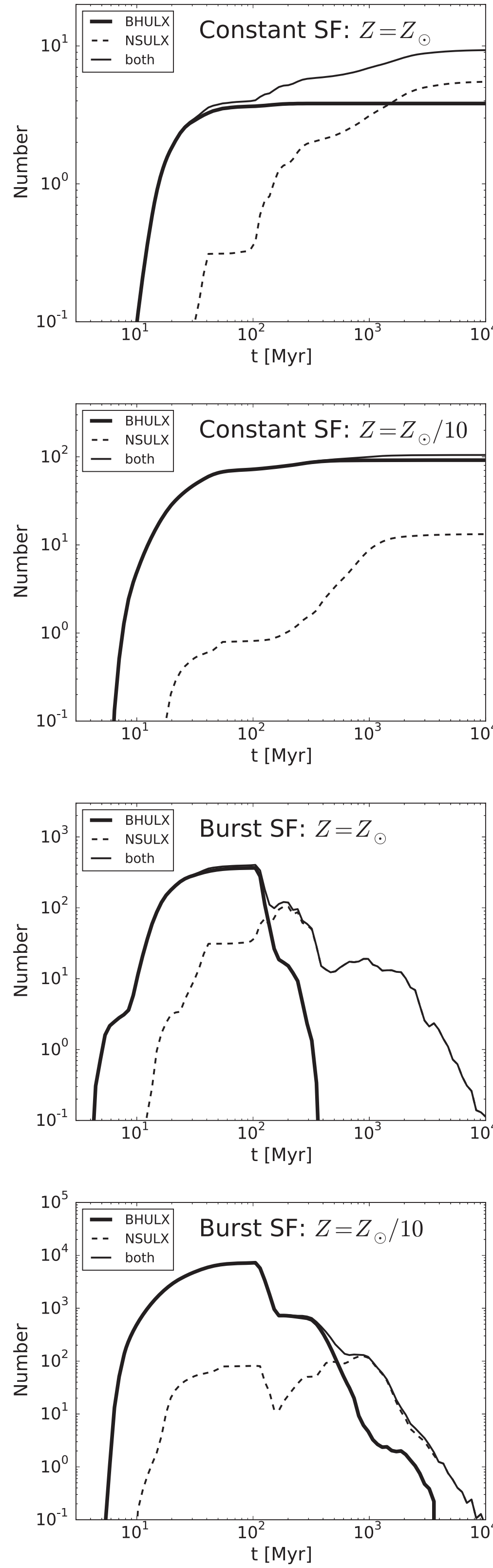

Figure 2. Time evolution of the number of ULXs since the beginning of star formation. The BHULXs (thick line) appear early, but 100–1000 Myr later the ULX population becomes dominated by the NSULXs (dashed line), except constant SF models with sub-solar metallicities. Number of ULXs for a star-forming mass of $6 \times 10^{10}\ M_\odot$ (see Section 2). Presented values are for all ULXs (including less typical routes, which are not presented in Table 1). For the relative abundance of young and old ULXs, see Figure 5.

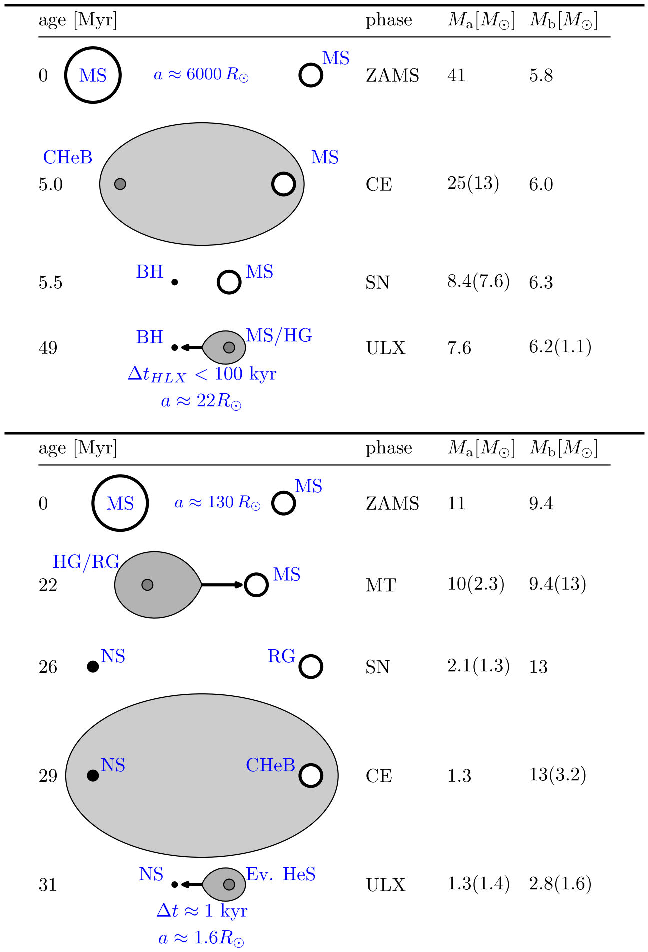

Figure 3. Similar to Figure 1, but for the evolution of the most luminous ($L_X > 10^{41}$ erg s^{-1}) ULXs. Top/bottom plot is for a BH/NS accretor.

galaxy ($M_{\rm MWEG} = 6 \times 10^{10}\,M_\odot$ (Licquia & Newman 2015); star-formation rate (SFR) equal 6.0 $M_\odot$ yr^{-1} for constant star formation (SF) during 10 Gyr, and 600 $M_\odot$ yr^{-1} for burst SF with a duration of 100 Myr). We do our study for solar metallicity ($Z_\odot$), 10% of solar ($Z_\odot/10$), and 1% of solar ($Z_\odot/100$).

2.1. Accretion Model

We implemented a model based on nonlinear scaling of X-ray luminosity and mass accretion rate (e.g., Shakura & Sunyaev 1973),

$$L_{\rm X,tot} = L_{\rm Edd}(1 + \ln \dot{m}), \tag{1}$$

where $\dot{m}$ is the mass transfer (MT) rate in Eddington rate units. Mass accretion onto the compact object ($\dot{M}_{\rm acc}$) is limited to $\dot{M}_{\rm Edd}$ and the rest of the mass transferred to the system is lost in a wind from the inner disk region. Such outflows from ULXs were recently observed by Pinto et al. (2016).

2.2. Beaming Model

The collimation of radiation from the innermost parts of the accretion disk, i.e., beaming, has a prodigious influence on the apparent isotropic luminosity. The beaming factor is defined as $b = \Omega/4\pi$, where Ω is the solid angle of emission (e.g., King et al. 2001). If we assume that there are two conical beams with opening angle θ, then $\Omega = 4\pi(1 - \cos\theta/2)$.

The isotropic equivalent X-ray luminosity (L_X) can be expressed as

$$L_X = \frac{L_{\rm X,tot}}{b}. \tag{2}$$

Under the assumption of the isotropic distribution of disk inclinations in space (see King 2009), the probability of observing a source along the beam is equal b.

The results of theoretical studies as well as the outcomes of detailed modeling of accretion disks favor the dependence of beaming on the MT rate (e.g., Lasota 2016). King (2009) proposed that b scales as

$$\begin{aligned} b &\sim \frac{73}{\dot{m}^2} \qquad \dot{m} \geqslant 8.5, \\ b &= 1 \qquad \dot{m} < 8.5. \end{aligned} \tag{3}$$

For very high MT rates, this prescription may give an extremely small value of b, i.e., strong beaming. For example, a Galactic ULX candidate SS433 has $\dot{m} \approx 3000$–10^4 (e.g., Fabrika 2004) for which Equations (3) and (2) give $b \approx 7 \times 10^{-7}$–$8 \times 10^{-6}$ and $L_X \approx 10^{46}$ erg s^{-1}. Therefore, we will assume saturation at $\dot{m} = 150$. For higher mass accretion rates, we will consider that the beaming is constant and equal $b \approx 3.2 \times 10^{-3}$ ($\theta \approx 9°$). Theoretical background for beaming saturation was presented by Lasota et al. (2016).

3. Results

In this section we provide results for the most typical systems and focus on the standard model (Section 2). In the Appendix, we provide additional characteristics of the simulated population of ULXs and results for other models.

3.1. Formation of NSULXs

According to our results, NSULX are present in ULX populations of all ages and metallicities. The first NSULXs form as early as ~6 Myr after the start of SF, but the ULX phase may occur also in a very old system ($t_{\rm age} \sim 5$ Gyr). Dominant evolutionary routes leading to the occurrence of high MT rate and formation of an NSULX depend on the age of the system at the time of the ULX phase. Below, we describe the typical routes for early ($\mathcal{R}_{\rm NS,MS}$), mid-age ($\mathcal{R}_{\rm NS,HG}$), and old ($\mathcal{R}_{\rm NS,RG}$) stellar populations (see also Figure 1). Ranges represent 50% of values in present day populations.[7]

6–59 Myr; *Route* $\mathcal{R}_{\rm NS,MS}$: *Typical companion MS*—On ZAMS, the masses of the primary and secondary are 7.2–12 $M_\odot$ and 1.3–2.0 $M_\odot$, respectively. The initial separation, 500–2600 $R_\odot$, shrinks during the CE phase commenced by the primary. After the CE phase, the primary forms an NS through a core collapse supernova explosion (SN). The natal kick leaves the system on an orbit that is tight enough for the secondary to fill its Roche lobe (RL) within about 2 kyr due to nuclear expansion and gravitational radiation (GR) before it leaves the main sequence (MS). During the RLOF, the companion is comparable in mass (0.9–1.5 $M_\odot$) to the NS (1.1–1.4 $M_\odot$), thus the MT is stable and may be sustained as long as ~1.3 Myr (see Figure 1, top).

400–820 Myr; *Route* $\mathcal{R}_{\rm NS,HG}$: *Typical companion HG*—In approximately 54%–73% percent of the systems following the

[7] For example, populations as we predict them to look for an observer able to see all the objects at the same time. Problems related to light propagation (e.g., light speed, interstellar absorption) are not discussed in this study.

Table 1
Typical Parameters of ULXs

	Present					ZAMS		
Route	t(Myr)	$\Delta\ t$(Myr)	$M_{\rm a}(M_\odot)$	$M_{\rm b}(M_\odot)$	$a(R_\odot)$	$M_{\rm ZAMS,a}(M_\odot)$	$M_{\rm ZAMS,b}(M_\odot)$	$a_{\rm ZAMS}(R_\odot)$
				$Z = Z_\odot$				
$\mathcal{R}_{\rm BH,MS}$	11–22	<0.2	7.7–8.6	5.9–7.2	18–22	40–50	6.6–12	3800–4600
ev. route: CE1(4-1; 7/8-1) SN1 MT2(14-1)								
$\mathcal{R}_{\rm NS,MS}$	6–38	$\lesssim$0.4	1.1–1.3	1.1–1.4	2.2–3.6	8.2–9.3	1.3–1.7	700–1200
ev. route: CE1(3/4/5-1; 7/8-1) SN1 MT2(13-1)								
$\mathcal{R}_{\rm NS,HG}$	430–730	0.3–0.8	~1.3	0.6–1.0	7.3–17	7.9–8.3	1.6–2.0	800–1200
ev. route: CE1(3/4/5-1; 7/8-1) SN1 MT2(13-1/2)								
$\mathcal{R}_{\rm NS,RG}$	2300–4300	0.1–0.2	~1.3	~1.0	35–50	7.5–7.9	1.2–1.5	1100–1700
ev. route: CE1(6-1; 12-1) MT2(12-3) AICNS1 MT2(13-3)								
				$Z = Z_\odot/10$				
$\mathcal{R}_{\rm BH,MS}$	4–37	<27	5.7–8.9	5.6–7.8	14–19	26–37	6.0–11	1800–3700
$\mathcal{R}_{\rm NS,MS}$	9–55	$\lesssim$0.8	1.1–1.3	1.2–1.5	1.6–2.7	7.2–12	1.5–1.9	1000–2600
$\mathcal{R}_{\rm NS,HG}$	400–820	$\lesssim$0.6	1.2–1.3	0.6–0.9	9.3–22	6–8	1.3–1.8	600–1500
$\mathcal{R}_{\rm NS,RG}$	1400–2600	$\lesssim$0.1	~1.3	~1.0	35–45	6.3–6.8	1.3–1.6	1700–2700
				$Z = Z_\odot/100$				
$\mathcal{R}_{\rm BH,MS}$	8.7–19	<1.0	12–21	7–11	12–17	35–55	9.1–14	540–2000
$\mathcal{R}_{\rm NS,MS}$	15–59	0.6–1.3	1.2–1.4	0.9–1.0	2.8–3.5	7.2–8.2	1.7–2.0	500–900
$\mathcal{R}_{\rm NS,HG}$	400–690	$\lesssim$0.4	~1.3	0.6–0.8	17–35	6.0–6.3	1.7–2.1	700–900
$\mathcal{R}_{\rm NS,RG}$	1200–2100	$\lesssim$0.1	~1.3	~1.0	30–45	6.0–6.2	1.3–1.7	900–1300

Note. Typical present and ZAMS parameters of most common ULX evolutionary routes. Ranges represent 50% of values in present day populations. The parameter columns represent, respectively: age of the system in ULX phase (t), duration of ULX phase (Δt), compact object mass ($M_{\rm a}$), donor mass ($M_{\rm b}$), separation (a), primary mass on ZAMS ($M_{\rm ZAMS,a}$), secondary mass on ZAMS ($M_{\rm ZAMS,b}$), separation on ZAMS ($a_{\rm ZAMS}$). The schematic evolutionary routes provided for $Z = Z_\odot$ are the same for other metallicities. Symbols represent (Belczynski et al. 2008) CE1—common envelope (donor: primary); MT2—mass transfer (donor: secondary); SN1—supernova (primary); AICNS1—accretion induced collapse (primary); 1—MS; 2—HG; 3—RG; 4—CHeB; 5—early AGB; 6—thermal-pulsing AGB; 7—HeS; 8—evHeS; 12—ONeWD; 13—NS; 14—BH.

Table 2
Typical Parameters of HLXs

	Present					ZAMS		
Route	t(Myr)	$\Delta\ t$(Myr)	$M_{\rm a}(M_\odot)$	$M_{\rm b}(M_\odot)$	$a(R_\odot)$	$M_{\rm ZAMS,a}(M_\odot)$	$M_{\rm ZAMS,b}(M_\odot)$	$a_{\rm ZAMS}(R_\odot)$
				$Z = Z_\odot$				
$\mathcal{R}_{\rm BH,HG}$	15–40	$\lesssim$0.08	8.0–10	1.7–3.3	20–90	40–50	3.8–8.2	3700–4600
ev. route CE1(4/5-1; 7/8-1) SN1 MT2(14-1/2)								
$\mathcal{R}_{\rm NS,evHeS}$	17–40	$\lesssim$0.001	1.3–1.4	1.7–2.6	$\lesssim$4.4	10–11	8.5–10	30–300
ev. route MT1(2/3/4/5/6-1/2/4) SN1 CE2(13-3/4/5; 13-7/8) MT2(13-8/9)								
				$Z = Z_\odot/10$				
$\mathcal{R}_{\rm BH,HG}$	20–60	$\lesssim$0.06	7.2–9.5	1.7–3.3	12–120	25–35	4.0–7.0	2000–5000
$\mathcal{R}_{\rm NS,evHeS}$	40–60	$\lesssim$0.001	~1.3	1.5–2.0	8.4–13	8.8–9.5	5.5–7.3	170–430
				$Z = Z_\odot/100$				
$\mathcal{R}_{\rm BH,HG}$	20–45	$\lesssim$0.04	10–18	1.2–3.7	10–75	25–45	5.0–9.0	700–2600
$\mathcal{R}_{\rm NS,evHeS}$	50–75	$\lesssim$0.001	~1.3	1.9–2.5	2.1–6.9	6.4–6.8	5.5–6.2	170–280

Note. Typical present and ZAMS parameters of typical most luminous ULXs (HLX; routes $\mathcal{R}_{\rm BH,HG}$ and $\mathcal{R}_{\rm NS,evHeS}$). The table is organized in the same way as Table 1.

$\mathcal{R}_{\rm NS,MS}$ route, the RLOF during the MS phase, if present, is not strong enough to power a ULX. These secondaries start to reach their terminal-age MS and expand rapidly several hundred Myr after the start of the SF. If the separation is short enough, they will fill their RL. Thus, at this time, a Hertzsprung-gap (HG) star becomes the most common NSULX companion.

1200–4300 Myr; *Route* $\mathcal{R}_{\rm NS,RG}$: *Typical companion RG*—The evolution of the late-time NSULXs is significantly different than that of the earlier ULXs. After a CE phase, the primary forms an oxygen–neon white dwarf (ONeWD) instead of an NS, and thus the mass of the primary is on average lower compared with routes $\mathcal{R}_{\rm NS,MS}$ and $\mathcal{R}_{\rm NS,HG}$. However, when the secondary becomes a red giant (RG) and fills its RL of ~10–20 $R_\odot$, the primary accretes additional mass and forms an NS due to an accretion induced collapse (AIC). Afterward, the RG refills its RL and a short ULX phase occurs (Figure 1, middle).

3.1.1. Formation of BHULXs

In general, BHULXs are a minority in our results. Nevertheless, they dominate the ULX population during the initial

Table 3
Frequently Used Abbreviations

ULX	Ultraluminous X-ray source
BHULX	ULX with a BH accretor
NSULX	ULX with an NS accretor
PULX	Pulsing ULX
MS	Main sequence
HG	H-rich Hertzsprung gap
RG	Red giant
CHeB	Core helium burning
HeS	Helium star
evHeS	Evolved helium star
SN	Supernova
AIC	Accretion induced collapse
RL	Roche lobe
RLOF	Roche lobe overFlow
MT	Mass transfer
GR	Gravitational radiation
SF	Star formation
WD	White dwarf
ONeWD	Oxygene–Neon WD

phase of the constant SF (the exception being populations with low ($\leqslant Z_{\odot}/10$) metallicity), and during the SF burst. They are also more numerous than NSULXs among the ULXs with luminosity in excess of 10^{41} erg s^{-1} (see Sections 3.2 and 3.3).

4–37 Myr; *Route* $\mathcal{R}_{\rm BH,MS}$: *Typical companion MS*—The initial binary on ZAMS consist of a massive primary (26–55 $M_{\odot}$) and an intermediate-mass secondary (6–14 $M_{\odot}$). The initial semimajor axis is $\sim$540–4000 $R_{\odot}$.

The heavier star evolves very quickly and during the CHeB phase fills its RL, commencing the CE episode. As a result, the primary is deprived of its hydrogen envelope and the separation drops to *a few* $\times$ 10 $R_{\odot}$. A direct collapse occurs shortly afterward. The combined action of the companion's nuclear expansion and GR leads to an RLOF. The phase of ULX emission is short, $\lesssim$1.0 Myr (Figure 1, bottom).

In the case of the $\mathcal{R}_{\rm BH,MS}$ channel, it is essential that the heavy primary expands and fills an RL of several $\times 100\ R_{\odot}$, which terminates the expansion. There may be some observational evidence that for the most massive stars ($M > 40\ M_{\odot}$) the large dimensions are avoided (Mennekens & Vanbeveren 2014). Additionally, the massive stars are almost all found in close interacting binaries (Sana et al. 2012), where very quickly their envelope is removed by RLOF and/or CE. It is naturally expected in our models. Since the post-MS expansion is very rapid ($\sim$200 kyr), and envelope removal is even quicker ($\sim$1 kyr) we do not expect many of the very massive stars to show up at a large radius (as red supergiants). Moreover, rapid rotation, which we do not take into account, may additionally limit the expansion of some of the most massive stars.

3.2. Number of ULXs

By the number of ULXs (#ULX), we understand the predicted number of observed systems at the present time. We find that #ULX strongly depends on the SFR history (Figure 2).

Constant SFR naturally leads to a constant growth in #ULX, which starts early after the start of SF ($\sim$5 Myr) and after a few gigayears reaches a constant value of #ULX = 9.3, 100, and 56 for $Z_{\odot}$, $Z_{\odot}/10$, and $Z_{\odot}/100$, respectively (see Section 4.2).

BHULXs appear first in both constant and burst SF scenarios. In the former case, the number of BHULXs increases to the age of a few hundred megayears, at which time it reaches a constant value of 3.8, 92, and 51 for $Z_{\odot}$, $Z_{\odot}/10$, and $Z_{\odot}/100$, respectively. In the case of a burst SF, the formation time of BHULXs is limited nearly exactly to the duration of the burst ($\lesssim$200 Myr).

NSULXs resulting from different evolutionary routes described in Section 3.1 appear sequentially in their chronological order and form the characteristic steep sections (constant SF) or humps (burst SF) at $\sim$100 Myr ($\mathcal{R}_{\rm NS,MS}$), $\sim$200 Myr ($\mathcal{R}_{\rm NS,HG}$), and $\sim$1 Gyr ($\mathcal{R}_{\rm NS,RG}$).

ULX populations younger than $\sim$100 Myr are dominated by the BHULX. For constant SF, the NSULXs become more abundant than the BHULXs (58% of the ULX accretors) only if $Z = Z_{\odot}$. For lower metallicities, the #BHULX grows rapidly during the first few hundred megayears, whereas the rate of the NSULXs formation is much lower, and they are not able to match the abundance of the BHULXs during the next 10 Gyr. As a result, the NSULXs account for not more than $\sim$12% and $\sim$8% of all ULXs for $Z_{\odot}/10$ and $Z_{\odot}/100$, respectively. However, for burst SF and all investigated metallicities, the NSULXs exceed the BHULXs in numbers within $\lesssim$1 Gyr, and after a few gigayears they become the only surviving ULXs.

3.3. ULXs with Luminosities Exceeding 10^{41} erg s^{-1}

Several surveys found a break in the X-ray luminosity function (XLF) at $\lesssim 2 \times 10^{10}$ erg s^{-1}, which may point toward different populations below and above this luminosity (e.g., Grimm et al. 2003; Swartz et al. 2011; Mineo et al. 2012). Thus, it is interesting to point out that hyper-luminous X-ray sources (HLX) defined as ULXs with $L_{\rm X} \gtrsim 10^{41}$ erg s^{-1}, thus clearly above the 2×10^{10} erg s^{-1} threshold, have different donors than the ULXs with $L_{\rm X} \ll 10^{41}$ erg s^{-1}. We find that 52%–84% of the ULXs (described in Section 3) have luminosities in the range of (1–3) $\times 10^{39}$ erg s^{-1}.

Approximately 90% of HLXs are BHULXs with HG donors. NS accretors in HLXs may obtain nearly as high luminosities as BH accretors and are typically accompanied by evolved helium stars (evHeS). It is noteworthy that the evolutionary HLX routes match those reported for HLXs with $L_{\rm X} \geqslant 10^{42}$ erg s^{-1} in Wiktorowicz et al. (2015). The current results, however, are based on a much wider range of models and a more physical treatment of NS/BH accretion, and we include here the HLX evolutionary paths for completeness (Table 2). Notice that the PULX NGC5907 ULX1 has a luminosity $\gtrsim 10^{41}$ erg s^{-1} (Fürst et al. 2016).

15–60 Myr; *Route* $\mathcal{R}_{\rm BH,HG}$: *Typical companion HG*—A typical system begins its evolution as a 25–50 $M_{\odot}$ primary with a 5–10 $M_{\odot}$ companion. After $\sim$5 Myr and the loss of 1–10 $M_{\odot}$ in stellar wind the primary fills the RL as a CHeB star and commences the CE phase. It loses a large fraction of its mass ($\sim$50%), but the separation shrinks to $\sim$15 $R_{\odot}$. After additional $\sim$0.5 Myr a $\sim$7–18 $M_{\odot}$ BH forms in a direct collapse. The secondary becomes an HG star $\sim$10–55 Myr later and it expands rapidly. Shortly after, it fills its RL and starts the MT. For a short time (<0.1 Myr), the MT is high enough to power a ULX with $L_{\rm X} > 10^{41}$ erg s^{-1} (see Figure 3, top).

17–75 Myr; *Route* $\mathcal{R}_{\rm NS,evHeS}$: *Typical companion evHeS*–The stars on ZAMS are less massive and have smaller mass ratios than in the case of $\mathcal{R}_{\rm BH,HG}$. When the primary fills the RL

Table 4
#ULX for Burst and Constant SFR

Metallicity		Time Since the Start of Star Formation				
		Burst SFR[a]				Constant SFR
		100 Myr	1 Gyr	5 Gyr	10 Gyr	10 Gyr
	#ULX	4.0×10^{2}	1.8×10^{1}	9.5×10^{-1}	1.1×10^{-1}	9.3×10^{0}
$Z_{\odot}$	#BHULX	3.7×10^{2}	2.8×10^{-7}	…	…	3.8×10^{0}
	#NSULX	3.5×10^{1}	1.8×10^{1}	9.5×10^{-1}	1.1×10^{-1}	5.5×10^{0}
	#ULX	7.3×10^{3}	1.1×10^{2}	7.0×10^{-1}	7.5×10^{-2}	1.0×10^{2}
$Z_{\odot}/10$	#BHULX	7.2×10^{3}	4.0×10^{0}	…	…	9.2×10^{1}
	#NSULX	8.1×10^{1}	1.1×10^{2}	7.0×10^{-1}	7.5×10^{-2}	1.3×10^{1}
	#ULX	5.0×10^{3}	2.9×10^{1}	1.0×10^{-1}	5.0×10^{-7}	5.6×10^{1}
$Z_{\odot}/100$	#BHULX	4.9×10^{3}	…	…	…	5.1×10^{1}
	#NSULX	1.6×10^{1}	2.9×10^{1}	1.0×10^{-1}	5.0×10^{-7}	5.0×10^{0}

Note. Number of ULXs (#ULX) in the reference model with a division on BHULXs (#BHULX) and NSULXs (#NSULX) for different population ages. BHULX are also present late after the burst (~1 Gyr), but #BHULX is negligible in that population's age in comparison to #NSULX or the #BHULX during the burst.
[a] Burst duration is 100 Myr.

Table 5
#ULX($L_{X,min}$) 100 Myr after SF Start

Metallicity		$L_{X,min}$			
		10^{39} erg s^{-1}	3×10^{39} erg s^{-1}	10^{40} erg s^{-1}	10^{41} erg s^{-1}
	#ULX	4.0×10^{2}	6.5×10^{1}	1.4×10^{1}	5.0×10^{-1}
$Z_{\odot}$	#BHULX	3.7×10^{2}	4.0×10^{1}	4.7×10^{0}	3.8×10^{-1}
	#NSULX	3.5×10^{1}	2.5×10^{1}	9.4×10^{0}	1.3×10^{-1}
	#ULX	7.3×10^{3}	1.9×10^{3}	2.0×10^{2}	1.2×10^{1}
$Z_{\odot}/10$	#BHULX	7.2×10^{3}	1.9×10^{3}	1.8×10^{2}	1.1×10^{1}
	#NSULX	8.1×10^{1}	4.0×10^{1}	1.2×10^{1}	4.3×10^{-1}
	#ULX	5.0×10^{3}	2.4×10^{3}	3.9×10^{2}	1.5×10^{1}
$Z_{\odot}/100$	#BHULX	4.9×10^{3}	2.4×10^{3}	3.8×10^{2}	1.5×10^{1}
	#NSULX	1.6×10^{1}	1.2×10^{1}	9.0×10^{0}	7.5×10^{-2}

Note. Number of ULXs depending on the minimal luminosity ($L_{X,min}$) for different metallicities with a division on BHULXs and NSULXs for AD1 BK model.

as an RG, the MT is stable and proceeds for a few tens of kyr. The donor losses most of its hydrogen envelope and after a few Myr at the age of ~25 Myr it forms an NS through an SN explosion. The companion, being an RG, expands and fills its RL. This time the MT is unstable due to a high-mass ratio and the CE occurs. Afterward, the secondary becomes a low-mass (a few Solar masses) helium star (HeS). The secondary continues its evolution for the next few Myr s, then expands and fills its RL again. This time, although being very strong, the MT is stable and for ~1 kyr it powers an HLX (see Figure 3, bottom).

4. Discussion

ULXs are observed in all kinds of galaxies (e.g., Mushotzky 2006). However, ULXs appear to be more abundant in the star-forming galaxies than in the elliptical galaxies (e.g., Irwin et al. 2004; Swartz et al. 2004; Feng & Soria 2011; Wang et al. 2016; however, see Soria 2007). In addition, ULXs are commonly detected in star-burst regions (e.g., Fabbiano et al. 2001; Gao et al. 2003). Feng & Soria (2011) pointed out that this connection is particularly valid for the most luminous ULXs. On the contrary, Mushotzky (2006) performed a direct examination of the ULXs' positions and found that approximately one-third of them had to form outside of the star-forming regions.

These observations may be understood on the ground of our results. On the one hand, the spatial correlation of ULXs and SF regions is expected because during the SF episodes ULXs form mainly through routes $\mathcal{R}_{BH,MS}$ and $\mathcal{R}_{NS,MS}$, which produce numerous sources early after the start of SF. Additionally, the most luminous ULXs (HLXs) formed in our simulations evolve from heavier stars at an early age ($t_{age} \lesssim 200$ Myr). On the other hand, the ULX phase in systems formed outside the SF regions occurs later on after ZAMS ($\mathcal{R}_{NS,HG}$, $\mathcal{R}_{NS,RG}$). However, we found that these late-time ULXs constitute only 1%–10% of all ULXs for constant SF.

4.1. NS Accretors in ULXs

Our results predict a large fraction of NS accretors among the ULXs. Current observational status is consistent with our results. The discovery of the first NSULX (Bachetti et al. 2014) proved

Table 6
Number of ULXs and Maximal Luminosity (Constant SFR[a])

Model[b]	Number per MWEG[c]			$L_{X,max}$ (erg s^{-1})[d]	
	#ULX	#BHULX	#NSULX	BHULX	NSULX
			$Z_\odot$		
AD0 BN	3.1×10^1	3.1×10^0 (10%)	2.8×10^1 (89%)	8.4×10^{44}	3.3×10^{44}
AD0 B01	1.8×10^2	1.1×10^0 (0%)	1.8×10^2 (99%)	8.4×10^{45}	3.3×10^{45}
AD0 BK	2.2×10^1	2.7×10^0 (12%)	1.9×10^1 (87%)	2.6×10^{47}	1.0×10^{47}
AD0 BS	2.0×10^1	2.3×10^0 (11%)	1.8×10^1 (88%)	5.5×10^{45}	2.2×10^{45}
AD1 BN	1.5×10^1	4.4×10^0 (29%)	1.1×10^1 (70%)	3.0×10^{40}	5.1×10^{39}
AD1 B01	2.0×10^2	1.5×10^0 (0%)	2.0×10^2 (99%)	3.0×10^{41}	5.1×10^{40}
AD1 BK	9.3×10^0	3.8×10^0 (41%)	5.5×10^0 (58%)	9.2×10^{42}	1.6×10^{42}
AD1 BS	2.0×10^1	2.9×10^0 (14%)	1.7×10^1 (85%)	2.0×10^{41}	3.4×10^{40}
			$Z_\odot/10$		
AD0 BN	1.6×10^2	9.4×10^1 (58%)	6.7×10^1 (41%)	6.8×10^{45}	2.3×10^{44}
AD0 B01	3.7×10^2	4.3×10^1 (11%)	3.3×10^2 (88%)	6.8×10^{46}	2.3×10^{45}
AD0 BK	1.3×10^2	8.4×10^1 (63%)	5.0×10^1 (36%)	2.1×10^{48}	7.1×10^{46}
AD0 BS	1.1×10^2	6.4×10^1 (60%)	4.1×10^1 (39%)	4.5×10^{46}	1.5×10^{45}
AD1 BN	1.3×10^2	1.1×10^2 (83%)	2.1×10^1 (16%)	8.6×10^{40}	4.5×10^{39}
AD1 B01	4.2×10^2	5.0×10^1 (11%)	3.7×10^2 (88%)	8.6×10^{41}	4.5×10^{40}
AD1 BK	1.0×10^2	9.2×10^1 (87%)	1.3×10^1 (12%)	2.7×10^{43}	1.4×10^{42}
AD1 BS	1.1×10^2	6.8×10^1 (61%)	4.2×10^1 (38%)	5.7×10^{41}	3.0×10^{40}
			$Z_\odot/100$		
AD0 BN	8.5×10^1	6.1×10^1 (72%)	2.3×10^1 (27%)	8.9×10^{45}	2.5×10^{44}
AD0 B01	8.6×10^1	1.4×10^1 (16%)	7.2×10^1 (83%)	8.9×10^{46}	2.5×10^{45}
AD0 BK	7.2×10^1	5.6×10^1 (78%)	1.6×10^1 (21%)	2.7×10^{48}	7.7×10^{46}
AD0 BS	4.9×10^1	3.8×10^1 (78%)	1.1×10^1 (21%)	5.9×10^{46}	1.6×10^{45}
AD1 BN	6.6×10^1	5.9×10^1 (89%)	7.2×10^0 (10%)	1.3×10^{41}	5.5×10^{39}
AD1 B01	8.0×10^1	1.6×10^1 (19%)	6.4×10^1 (80%)	1.3×10^{42}	5.5×10^{40}
AD1 BK	5.6×10^1	5.1×10^1 (91%)	5.0×10^0 (8%)	4.0×10^{43}	1.7×10^{42}
AD1 BS	5.0×10^1	3.7×10^1 (73%)	1.3×10^1 (26%)	8.6×10^{41}	3.6×10^{40}

Notes.
[a] At the age of 10 Gyr.
[b] AD0/1—"upper limit"/logarythmic accretion model (Appendix A.1 and Section 2.1); BN/B01/BK/BS—beaming models (Appendix A.2 and Section 2.2).
[c] Milky Way Equivalent Galaxy.
[d] The maximal obtained luminosity for the particular accretor. In all cases, the beaming that corresponds to these luminosities is saturated, so the beaming factor $b = 1$, 0.1, $\sim 3.2 \times 10^{-3}$, and ~ 0.15 for BN, B01, BK, and BS, respectively. Corresponding opening angles are 180°, ∼52°, ∼9°, and ∼64°, respectively.

that apparent luminosities orders of magnitude larger than the EL are possible in nature. Kluźniak & Lasota (2015) proposed that the M82 X-1 and the P13 in NGC 7793 may also be PULXs. The following discoveries (Fürst et al. 2016; Israel et al. 2017a) showed that NSs may indeed be widespread among the ULXs. Finally, a known X-ray pulsar SMC X-3 was reported to reach an outburst luminosity of 2.5×10^{39} erg s^{-1} (Tsygankov et al. 2017). Pintore et al. (2017) argued that the energy spectra of several ULXs can be explained with a "pulsator-like" continuum model used to describe Galactic XRBs containing NSs (e.g., White et al. 1995; Coburn et al. 2001).

Theoretical considerations further support our findings. King & Lasota (2016) showed that a ULX with a weakly magnetized NS and a ULX with a BH may be observationally hard to distinguish if the NS does not pulsate. King et al. (2017) argued that the conditions for pulsations in PULXs are relatively strict and a large population of NSULXs will mimic the BHULXs.

The significant number of NSULX that follows from most of our simulated models may be understood on the statistical ground. While it is easier to obtain large MT rates in the BHULXs, the NSULXs progenitors are more abundant in the ZAMS distributions. In general, NSs form from stars with ZAMS masses ~ 8–$22\,M_\odot$, whereas BHs form from more massive stars with ~ 22–$150\,M_\odot$. For $\alpha_{IMF} = -2.7$, it gives the ratio of NS to BH progenitors of ∼4.8, and for $\alpha_{IMF} = -2.3$ this ratio is 3.0. Moreover, in the NSULX route, which dominates in the old stellar populations ($\mathcal{R}_{NS,RG}$), the primary on ZAMS may have an even lower mass of $\sim 6\,M_\odot$, which gives the ratio of NS to BH progenitors of 4.8 for $\alpha_{IMF} = -2.3$. It first becomes a WD before accreting mass and collapsing into an NS. Additionally, donors in NSULXs are less massive than in BHULXs and, therefore, also more abundant on ZAMS. We note that low-mass donors may occur also in BHULXs, but it is far harder (and therefore less probable) for them to survive the CE. Even if they succeeded, the post-CE separation is so small that the RLOF occurs earlier than what is typical for NSULXs. All of these results are for a significantly smaller number of BHULXs with low-mass ($\lesssim 2\,M_\odot$) donors than in NSULXs.

During short SF episodes, the ULX population is dominated by sources with BH accretors. BHs may acquire stable MT from heavier companions than NSs. Heavier stars expand more and faster, therefore, BHULXs age during ULX phase is of the order of ∼10 Myr, whereas for NSULX it is ∼100 Myr (route

Table 7
General Parameters of the Simulational Results (Burst SFR 100 Myr Ago)

Model[a]	Number per MWEG[a]			$L_{X,max}$ (erg s^{-1})[b]	
	#ULX	#BHULX	#NSULX	BHULX	NSULX
			$Z_\odot$		
AD0 BN	3.4×10^2	2.8×10^2 (83%)	5.8×10^1 (16%)	8.4×10^{44}	3.3×10^{44}
AD0 B01	4.7×10^2	9.3×10^1 (19%)	3.8×10^2 (80%)	8.4×10^{45}	3.3×10^{45}
AD0 BK	2.8×10^2	2.6×10^2 (90%)	2.8×10^1 (9%)	2.6×10^{47}	1.0×10^{47}
AD0 BS	2.8×10^2	2.1×10^2 (75%)	6.8×10^1 (24%)	5.5×10^{45}	2.2×10^{45}
AD1 B01	5.7×10^2	1.3×10^2 (22%)	4.4×10^2 (77%)	3.0×10^{41}	5.1×10^{40}
AD1 BK	4.0×10^2	3.7×10^2 (91%)	3.5×10^1 (8%)	9.2×10^{42}	1.6×10^{42}
AD1 BS	3.8×10^2	2.8×10^2 (75%)	9.4×10^1 (24%)	2.0×10^{41}	3.4×10^{40}
			$Z_\odot/10$		
AD0 BN	7.5×10^3	7.2×10^3 (96%)	2.9×10^2 (3%)	6.8×10^{45}	1.2×10^{44}
AD0 B01	3.0×10^3	3.0×10^3 (98%)	4.9×10^1 (1%)	6.8×10^{46}	1.2×10^{45}
AD0 BK	6.6×10^3	6.4×10^3 (98%)	1.2×10^2 (1%)	2.1×10^{48}	3.7×10^{46}
AD0 BS	5.2×10^3	5.1×10^3 (98%)	6.7×10^1 (1%)	4.5×10^{46}	7.9×10^{44}
AD1 BN	8.6×10^3	8.5×10^3 (98%)	1.0×10^2 (1%)	8.6×10^{40}	4.5×10^{39}
AD1 B01	3.9×10^3	3.8×10^3 (96%)	1.4×10^2 (3%)	8.6×10^{41}	4.5×10^{40}
AD1 BK	7.3×10^3	7.2×10^3 (98%)	8.1×10^1 (1%)	2.7×10^{43}	1.4×10^{42}
AD1 BS	5.7×10^3	5.6×10^3 (97%)	1.5×10^2 (2%)	5.7×10^{41}	3.0×10^{40}
			$Z_\odot/100$		
AD0 BN	5.9×10^3	5.9×10^3 (99%)	2.8×10^1 (0%)	8.9×10^{45}	2.1×10^{43}
AD0 B01	1.3×10^3	1.3×10^3 (99%)	4.4×10^0 (0%)	8.9×10^{46}	2.1×10^{44}
AD0 BK	5.4×10^3	5.4×10^3 (99%)	1.1×10^1 (0%)	2.7×10^{48}	6.5×10^{45}
AD0 BS	3.7×10^3	3.7×10^3 (99%)	6.9×10^0 (0%)	5.9×10^{46}	1.4×10^{44}
AD1 BN	5.7×10^3	5.7×10^3 (99%)	1.4×10^1 (0%)	1.3×10^{41}	5.5×10^{39}
AD1 B01	1.5×10^3	1.5×10^3 (96%)	4.9×10^1 (3%)	1.3×10^{42}	5.5×10^{40}
AD1 BK	5.0×10^3	4.9×10^3 (99%)	1.6×10^1 (0%)	4.0×10^{43}	1.7×10^{42}
AD1 BS	3.7×10^3	3.6×10^3 (98%)	5.8×10^1 (1%)	8.6×10^{41}	3.6×10^{40}

Note. The same as in Table 6, but for burst SF, which started 100 Myr ago and lasted for 100 Myr.

$\mathcal{R}_{NS,MS}$). As a result BHULXs appear in larger numbers in the first $\sim$100 Myr. The ULX phase may appear in NSULX as early as $\sim$10 Myr after ZAMS. However, it demands a very specific pre-CE conditions, which occur in a relatively narrow ZAMS parameter space. For an average post-CE separation in early NSULXs ($\mathcal{R}_{NS,MS}$) the star needs $\sim$100 Myr to fill its RL.

The picture is different for the constant SF or long bursts. As the SF continues, the #BHULX saturates for $\sim$200 Myr after the SF start, because at this time a comparable number of sources begin and end their ULX phase. However, a significant number of NSULXs have their ULX phases during the post-MS expansion of their light donors. Therefore, the #NSULX grows continuously for several gigayears and new NSULX formation routes appear successively (see Section 3.1 for the sequence). For $Z = Z_\odot$, the #NSULX becomes higher than #BHULX after $\sim$1 Gyr. However, for lower metallicities, #NSULX does not overcome #BHULX within 10 Gyr.

When the SF is extinguished, $\mathcal{R}_{BH,MS}$ quickly disappear as their massive donors quickly end their lives ($\lesssim$500 Myr). On the other hand, NSULXs with low-mass donors may commence the ULX phase after several gigayears of evolution when the secondary fills the RL during the post-MS expansion ($\mathcal{R}_{NS,HG}$ and $\mathcal{R}_{NS,RG}$). Therefore, after the end of the SF, NSULXs quickly (in $\sim$100 Myr) become the dominant ULXs and after $\sim$1 Gyr BHULXs disappear completely.

The population synthesis of NSULXs was recently performed with the use of the BSE code by Fragos et al. (2015). However, they omitted the pre-SN evolution and explored a far smaller parameter space than that presented in this work. Even though they utilized the MESA code to calculate the MT rates, their maximum values are similar to ours ($\dot{M} \lesssim 10^{-2}$ Myr). We obtained less massive companions in NSULXs, but (Fragos et al. 2015) focused on M82 X-2 source with companion mass $\gtrsim$5.2 $M_\odot$ (Bachetti et al. 2014) and assumed that heavier stars are necessary to survive the CE phase.

Shao & Li (2015) also took the population synthesis approach to study NSULXs and found a significant population of these sources. They adopted a realistic envelope's binding energy from Xu & Li (2010), but considered only a solar metallicity and constant beaming of $b = 0.1$.

4.2. Dependence of #ULX on Metallicity

Observations show that ULXs are often associated with low metallicity environments (e.g., Pakull & Mirioni 2002; Soria et al. 2005; Luangtip et al. 2015; Mapelli et al. 2010). Many authors have demonstrated that in a low metallicity environment it is easier to form a massive BH (e.g., Mapelli et al. 2009; Zampieri & Roberts 2009; Belczynski et al. 2010), and it is more common to obtain an RLOF onto a compact object (Linden et al. 2010).

In this study, we find that the metallicity has a strong impact on #ULX, but only in SF regions (See Table 4). We show that the number of #BHULX increases significantly for $Z_\odot/10$ in comparison to $Z_\odot$. However, the #NSULX is virtually unaffected by metallicity. Interestingly, for models with the lowest investigated metallicity ($Z_\odot/100$), we found fewer ULXs than for $Z = Z_\odot/10$. Therefore, our results suggest that

Table 8
General Parameters of the Simulational Results (Burst SFR 1 Gyr Ago)

Model[a]	Number per MWEG[a]			$L_{X,max}$ (erg s^{-1})[b]	
	#ULX	#BHULX	#NSULX	BHULX	NSULX
			$Z_{\odot}$		
AD0 BN	8.3×10^1	8.5×10^{-3} (0%)	8.3×10^1 (99%)	2.0×10^{42}	2.2×10^{42}
AD0 B01	3.9×10^2	3.6×10^{-1} (0%)	3.9×10^2 (99%)	2.0×10^{43}	2.2×10^{43}
AD0 BK	6.0×10^1	3.5×10^{-4} (0%)	6.0×10^1 (99%)	6.2×10^{44}	6.8×10^{44}
AD0 BS	5.5×10^1	1.5×10^{-3} (0%)	5.5×10^1 (99%)	1.3×10^{43}	1.4×10^{43}
AD1 BN	3.8×10^1	8.7×10^{-5} (0%)	3.8×10^1 (99%)	3.7×10^{39}	3.9×10^{39}
AD1 B01	5.2×10^2	1.2×10^{-1} (0%)	5.2×10^2 (99%)	3.7×10^{40}	3.9×10^{40}
AD1 BK	1.8×10^1	2.8×10^{-7} (0%)	1.8×10^1 (99%)	1.1×10^{42}	1.2×10^{42}
AD1 BS	8.0×10^1	1.3×10^{-5} (0%)	8.0×10^1 (99%)	2.4×10^{40}	2.6×10^{40}
			$Z_{\odot}/10$		
AD0 BN	6.8×10^2	4.1×10^0 (0%)	6.8×10^2 (99%)	4.8×10^{42}	1.4×10^{43}
AD0 B01	8.5×10^2	1.2×10^1 (1%)	8.4×10^2 (98%)	4.8×10^{43}	1.4×10^{44}
AD0 BK	5.7×10^2	3.9×10^0 (0%)	5.7×10^2 (99%)	1.5×10^{45}	4.3×10^{45}
AD0 BS	2.8×10^2	4.2×10^0 (1%)	2.8×10^2 (98%)	3.2×10^{43}	9.2×10^{43}
AD1 BN	1.2×10^2	4.0×10^0 (3%)	1.2×10^2 (96%)	9.0×10^{39}	3.5×10^{39}
AD1 B01	9.9×10^2	5.0×10^0 (0%)	9.8×10^2 (99%)	9.0×10^{40}	3.5×10^{40}
AD1 BK	1.1×10^2	4.0×10^0 (3%)	1.1×10^2 (96%)	2.8×10^{42}	1.1×10^{42}
AD1 BS	2.9×10^2	3.8×10^0 (1%)	2.9×10^2 (98%)	5.9×10^{40}	2.3×10^{40}
			$Z_{\odot}/100$		
AD0 BN	2.2×10^2	5.6×10^{-2} (0%)	2.2×10^2 (99%)	3.4×10^{42}	7.3×10^{42}
AD0 B01	1.7×10^2	1.6×10^0 (0%)	1.7×10^2 (99%)	3.4×10^{43}	7.3×10^{43}
AD0 BK	1.6×10^2	1.3×10^{-2} (0%)	1.6×10^2 (99%)	1.0×10^{45}	2.2×10^{45}
AD0 BS	7.2×10^1	1.1×10^{-2} (0%)	7.2×10^1 (99%)	2.2×10^{43}	4.8×10^{43}
AD1 BN	3.1×10^1	0.0×10^0 (0%)	3.1×10^1 (100%)	0.0×10^0	2.8×10^{39}
AD1 B01	2.2×10^2	0.0×10^0 (0%)	2.2×10^2 (100%)	0.0×10^0	2.8×10^{40}
AD1 BK	2.9×10^1	0.0×10^0 (0%)	2.9×10^1 (100%)	0.0×10^0	8.6×10^{41}
AD1 BS	6.3×10^1	0.0×10^0 (0%)	6.3×10^1 (100%)	0.0×10^0	1.8×10^{40}

Note. The same as in Table 6, but for burst SF, which started 1 Gyr ago and lasted for 100 Myr.

the relation #ULX(Z) is not monotonic (see Prestwich et al. 2013). We plan to study this outcome in more detail in a forthcoming publication (G. Wiktorowicz et al. 2017, in preparation).

4.3. Counterparts

Several searches were performed to directly observe the ULX companions. However, only a handful have been detected among hundreds of known ULXs. Additionally, ULXs, being extra-galactic objects, are observationally biased toward more luminous and therefore more massive companions. In our results, NS counterparts in ULX are predominantly low-mass ($\lesssim 1.5\,M_{\odot}$) stars. If located in other galaxies, such objects would be difficult to detect. This may explain why it is hard to find counterparts to the majority of the ULXs.

Some ULXs were observed near OB stars (e.g., Soria et al. 2005). Such stars are too massive to provide a stable MT to an NS accretor, so they may only be accompanied by BH accretors, unless the MT occurs through a stellar wind (not considered in our study). OB stars evolve quickly (<100 Myr), which suggests that they should be spatially associated with the SF regions, where the BHULXs are more numerous than the NSULXs according to our results. Typical BHULX companions in our simulations are MS stars of 5.6–11 $M_{\odot}$, which matches the B spectral type.

Roberts et al. (2008) found five potential optical ULX companions with the use of the *Hubble Space Telescope*. The optical search for companions in ULXs was performed also by Gladstone et al. (2013) who used the same instrument and found 13 ± 5 counterparts to ULXs located within a distance of $D \leqslant 5$ Mpc. Most of them were MS stars or RGs. A near-infrared search was performed by Heida et al. (2014, 2016) who observed 62 ULXs in 37 galaxies located within 10 Mpc. They found 17 candidate counterparts, 13 of which are red supergiants. We note that red supergiants are present in our results in small numbers (<1%). The relatively large number of these stars in observations may be an observational bias, as they are significantly brighter than the most typical companions predicted by our study (<2 $M_{\odot}$). Nevertheless, red supergiants may be an interesting topic for a separate study.

The companion to NSULX P13 in NGC 7793 was detected and estimated to be a BI9a star with mass 18–23 $M_{\odot}$ (Motch et al. 2014). The radius of such a star is 4–700 $R_{\odot}$, depending on its evolutionary stage. An orbital period estimate ($P_{orb} = 64$ days) puts an RL radius of a donor at $\sim 120\,R_{\odot}$ (under the assumption of circular orbit and $M_{NS} = 1.4\,M_{\odot}$). The BI9a star may obtain such a radius during the CHeB phase. According to a standard prescription, in a high mass-ratio system, the RLOF will be unstable and the CE will occur. However, Pavlovskii et al. (2017) found that the range of stable mass ratios may be wider than previously thought. We will analyze this possibility in a separate study (Wiktorowicz et al. 2017, in preparation). BHULXs with high-mass donors may be predecessors of double BH mergers (Belczynski et al. 2016).

Table 9
General Parameters of the Simulational Results (Burst SFR 5 Gyr Ago)

Model[a]	Number per MWEG[a]			$L_{X,max}$ (erg s^{-1})[b]	
	#ULX	#BHULX	#NSULX	BHULX	NSULX
			$Z_{\odot}$		
AD0 BN	7.3×10^{0}	0.0×10^{0} (0%)	7.3×10^{0} (100%)	0.0×10^{0}	7.2×10^{43}
AD0 B01	6.6×10^{1}	0.0×10^{0} (0%)	6.6×10^{1} (100%)	0.0×10^{0}	7.2×10^{44}
AD0 BK	4.9×10^{0}	0.0×10^{0} (0%)	4.9×10^{0} (100%)	0.0×10^{0}	2.2×10^{46}
AD0 BS	3.5×10^{0}	0.0×10^{0} (0%)	3.5×10^{0} (100%)	0.0×10^{0}	4.7×10^{44}
AD1 BN	7.2×10^{-1}	0.0×10^{0} (0%)	7.2×10^{-1} (100%)	0.0×10^{0}	2.9×10^{39}
AD1 B01	5.0×10^{1}	0.0×10^{0} (0%)	5.0×10^{1} (100%)	0.0×10^{0}	2.9×10^{40}
AD1 BK	9.5×10^{-1}	0.0×10^{0} (0%)	9.5×10^{-1} (100%)	0.0×10^{0}	8.9×10^{41}
AD1 BS	2.0×10^{0}	0.0×10^{0} (0%)	2.0×10^{0} (100%)	0.0×10^{0}	1.9×10^{40}
			$Z_{\odot}/10$		
AD0 BN	6.7×10^{0}	0.0×10^{0} (0%)	6.7×10^{0} (100%)	0.0×10^{0}	9.4×10^{42}
AD0 B01	6.5×10^{1}	7.2×10^{-1} (1%)	6.4×10^{1} (98%)	6.1×10^{39}	9.4×10^{43}
AD0 BK	4.9×10^{0}	0.0×10^{0} (0%)	4.9×10^{0} (100%)	0.0×10^{0}	2.9×10^{45}
AD0 BS	4.4×10^{0}	0.0×10^{0} (0%)	4.4×10^{0} (100%)	0.0×10^{0}	6.2×10^{43}
AD1 BN	1.4×10^{0}	0.0×10^{0} (0%)	1.4×10^{0} (100%)	0.0×10^{0}	3.0×10^{39}
AD1 B01	5.1×10^{1}	0.0×10^{0} (0%)	5.1×10^{1} (100%)	0.0×10^{0}	3.0×10^{40}
AD1 BK	7.0×10^{-1}	0.0×10^{0} (0%)	7.0×10^{-1} (99%)	0.0×10^{0}	9.2×10^{41}
AD1 BS	3.2×10^{0}	0.0×10^{0} (0%)	3.2×10^{0} (100%)	0.0×10^{0}	2.0×10^{40}
			$Z_{\odot}/100$		
AD0 BN	1.9×10^{0}	0.0×10^{0} (0%)	1.9×10^{0} (100%)	0.0×10^{0}	1.2×10^{43}
AD0 B01	1.9×10^{1}	2.0×10^{-2} (0%)	1.9×10^{1} (99%)	6.8×10^{39}	1.2×10^{44}
AD0 BK	1.4×10^{0}	0.0×10^{0} (0%)	1.4×10^{0} (100%)	0.0×10^{0}	3.7×10^{45}
AD0 BS	2.0×10^{0}	0.0×10^{0} (0%)	2.0×10^{0} (100%)	0.0×10^{0}	7.9×10^{43}
AD1 BN	3.0×10^{-4}	0.0×10^{0} (0%)	3.0×10^{-4} (100%)	0.0×10^{0}	3.0×10^{39}
AD1 B01	4.9×10^{0}	1.2×10^{-1} (2%)	4.8×10^{0} (97%)	6.5×10^{39}	3.0×10^{40}
AD1 BK	1.0×10^{-1}	0.0×10^{0} (0%)	1.0×10^{-1} (100%)	0.0×10^{0}	9.2×10^{41}
AD1 BS	7.9×10^{-1}	0.0×10^{0} (0%)	7.9×10^{-1} (100%)	0.0×10^{0}	2.0×10^{40}

Note. The same as in Table 6, but for burst SF which started 5 Gyr ago and lasted for 100 Myr.

5. Summary and Conclusions

We analyzed accretion onto compact stars in order to investigate the parameters and characteristics of the ULX population. We demonstrate that on the grounds of the current understanding of the accretion physics and stellar evolution we are able to reproduce the vast majority of the observed population of ULXs without the need for intermediate-mass black hole accretors.

We performed a population synthesis study with the use of the StarTrack population synthesis code to simulate 2×10^{7} isolated binaries with initial parameters leading to the formation of XRBs (both LMXB and HMXB). Our simulation grid involves various accretion models, beaming prescriptions, and metallicities.

Our main conclusions are as follows.

(1) *ULX with NS accretors dominate the post-burst ULX populations,* and constant SF (duration >1 Gyr) in high-Z environments, which is a natural consequence of the current understanding of the binary evolution. NSULXs are present in significant numbers ($\gtrsim$10%) also during the SF bursts and in lower-Z ULX populations.

(2) *ULXs appear in a very specific sequence after the start of the SF* (t depicts here the time since the beginning of the SF):
1. $t \approx$ 4–40 Myr BH–MS (5.6–11 $M_{\odot}$),
2. $t \approx$ 6–800 Myr NS–MS (0.9–1.5 $M_{\odot}$),
3. $t \approx$ 430–1100 Myr NS–HG (0.6–1.0 $M_{\odot}$),
4. $t \approx$ 540–4400 Myr NS–RG ($\sim$1.0 $M_{\odot}$).

(3) *We found that NSULXs may reach luminosities as high as those of BHULXs* ($L_{X,max} > 10^{41}$ erg s^{-1}).

(4) *The most luminous ULXs* ($L_X \gtrsim 10^{41}$ erg s^{-1}) *contain HG donors* (BHULXs; $M_b \approx$ 1.2–3.7 $M_{\odot}$) *or evolved helium stars* (NSULXs; $M_b \approx$ 1.7–2.6 $M_{\odot}$), which overfill their RL and transfer mass on thermal-timescale. They form typically within 15–75 Myr since ZAMS.

(5) *The number of ULXs is anti-correlated with metallicity.* However, for very low-Z this relation changes sign.

We would like to thank volunteers whose participation in the Universe@Home project[8] made it possible to acquire the results in such a short time and the anonymous referee who helped to significantly improve the paper. G.W. and K.B. would like to thank W. Kluzniak for interesting discussions. This study was partially supported by the Polish National Science Center NCN grants: N203 404939, OPUS 2015/19/B/ST9/01099, and SONATA BIS 2 DEC-2012/07/E/ST9/01360. M.S. was supported by NASA contract NAS8-03060 (*Chandra* X-ray Center). M.S. also acknowledges the Polish NCN grant OPUS 2014/13/B/ST9/00570. J.P.L. was supported in part by a grant from the French National Space Center CNES. K.B. acknowledges support from the NCN grants: OPUS 2015/19/B/ST9/03188 and MAESTRO 2015/18/A/ST9/00746. G.W. was supported by the NCN grant OPUS 2015/19/B/ST9/03188 and HARMONIA 2014/14/M/ST9/

[8] http://universeathome.pl

Table 10
General Parameters of the Simulational Results (Burst SFR 10 Gyr Ago)

Model[a]	Number per MWEG[a]			$L_{X,max}$ (erg s^{-1})[b]	
	#ULX	#BHULX	#NSULX	BHULX	NSULX
			$Z_\odot$		
AD0 BN	1.2×10^0	0.0×10^0 (0%)	1.2×10^0 (100%)	0.0×10^0	8.7×10^{42}
AD0 B01	8.1×10^0	0.0×10^0 (0%)	8.1×10^0 (100%)	0.0×10^0	8.7×10^{43}
AD0 BK	8.3×10^{-1}	0.0×10^0 (0%)	8.3×10^{-1} (100%)	0.0×10^0	2.7×10^{45}
AD0 BS	7.4×10^{-1}	0.0×10^0 (0%)	7.4×10^{-1} (100%)	0.0×10^0	5.7×10^{43}
AD1 BN	2.9×10^{-2}	0.0×10^0 (0%)	2.9×10^{-2} (100%)	0.0×10^0	3.0×10^{39}
AD1 B01	2.6×10^0	0.0×10^0 (0%)	2.6×10^0 (100%)	0.0×10^0	3.0×10^{40}
AD1 BK	1.1×10^{-1}	0.0×10^0 (0%)	1.1×10^{-1} (100%)	0.0×10^0	9.2×10^{41}
AD1 BS	3.6×10^{-1}	0.0×10^0 (0%)	3.6×10^{-1} (100%)	0.0×10^0	2.0×10^{40}
			$Z_\odot/10$		
AD0 BN	1.5×10^0	0.0×10^0 (0%)	1.5×10^0 (100%)	0.0×10^0	5.4×10^{42}
AD0 B01	1.2×10^1	0.0×10^0 (0%)	1.2×10^1 (100%)	0.0×10^0	5.4×10^{43}
AD0 BK	1.1×10^0	0.0×10^0 (0%)	1.1×10^0 (100%)	0.0×10^0	1.7×10^{45}
AD0 BS	9.4×10^{-1}	0.0×10^0 (0%)	9.4×10^{-1} (100%)	0.0×10^0	3.6×10^{43}
AD1 BN	2.1×10^{-1}	0.0×10^0 (0%)	2.1×10^{-1} (100%)	0.0×10^0	2.8×10^{39}
AD1 B01	7.3×10^0	0.0×10^0 (0%)	7.3×10^0 (100%)	0.0×10^0	2.8×10^{40}
AD1 BK	7.5×10^{-2}	0.0×10^0 (0%)	7.5×10^{-2} (100%)	0.0×10^0	8.6×10^{41}
AD1 BS	2.9×10^{-1}	0.0×10^0 (0%)	2.9×10^{-1} (100%)	0.0×10^0	1.8×10^{40}
			$Z_\odot/100$		
AD0 BN	6.2×10^{-1}	0.0×10^0 (0%)	6.2×10^{-1} (100%)	0.0×10^0	5.1×10^{42}
AD0 B01	5.9×10^0	0.0×10^0 (0%)	5.9×10^0 (100%)	0.0×10^0	5.1×10^{43}
AD0 BK	4.4×10^{-1}	0.0×10^0 (0%)	4.4×10^{-1} (100%)	0.0×10^0	1.6×10^{45}
AD0 BS	3.8×10^{-1}	0.0×10^0 (0%)	3.8×10^{-1} (100%)	0.0×10^0	3.4×10^{43}
AD1 BN	1.5×10^{-4}	0.0×10^0 (0%)	1.5×10^{-4} (100%)	0.0×10^0	2.8×10^{39}
AD1 B01	2.9×10^0	0.0×10^0 (0%)	2.9×10^0 (100%)	0.0×10^0	2.8×10^{40}
AD1 BK	5.0×10^{-7}	0.0×10^0 (0%)	5.0×10^{-7} (100%)	0.0×10^0	8.6×10^{41}
AD1 BS	2.3×10^{-5}	0.0×10^0 (0%)	2.3×10^{-5} (100%)	0.0×10^0	1.8×10^{40}

Note. The same as in Table 6, but for burst SF, which started 10 Gyr ago and lasted for 100 Myr. A total absence of BHULXs may be observed.

0707. This research was supported in part by the National Science Foundation under grant No. NSF PHY-1125915.

Appendix
Details of the Simulations

If not stated differently, throughout the article a "luminosity" means an X-ray luminosity in the 0.2–10 keV band. We do not take into account NS magnetic fields and include only non-rotating BHs. All of the frequently used abbreviations are summarized in Table 3.

We utilized the EL for luminosity ($L_{\rm Edd}$) and mass accretion ($\dot{M}_{\rm Edd}$) as

$$L_{\rm Edd} = \eta\, \dot{M}_{\rm Edd} c^2 = 2.51 \times 10^{38}\ {\rm erg\ s^{-1}} \frac{1}{1+X}\left(\frac{\dot{M}_{\rm acc}}{M_\odot}\right), \quad (4)$$

where $\eta = 1/12$ for BH accretors and $\sim$0.2 for NSs, X is a fraction of hydrogen in the envelope of the donor. $X = 0.7$ for hydrogen reach donors and $X = 0$ for HeS and WD.

Most of the results are provided as present time distributions. This means the distributions as they will be visible by an observer in present time (10 Gyr after the SF beginning for constant SF, or (100 Myr, 1 Gyr, 5 Gyr, and 10 Gyr after the SF beginning for burst SF). We omit issues related to obscuration or light propagation time.

Below, we list the additional models tested in our grid of simulations. The standard model will be referred to as AD1 BK.

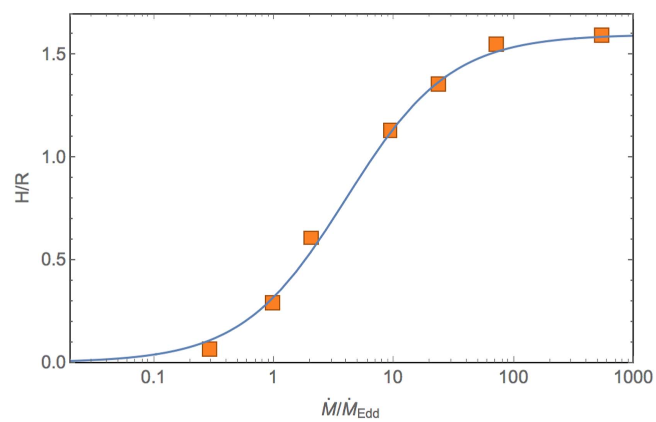

Figure 4. Ratio of photosphere height to disk radius (H/R) in relation to the mass transfer rate (in Eddington units). Orange squares represent the results of GRRMHD simulations with the use of KORAL code (A. Sądowski et al. 2016, private communication). The blue line shows the fit to the data (Equation (8)).

A.1. The "Upper Limit" Accretion Model (AD0)

In addition to the accretion model described in Section 2.1, to which we will refer to as AD1, we investigated a possibility that all mass may be transferred from the donor and efficiently accreated by the accretor, i.e.,

$$\dot{M}_{\rm acc} = \dot{M}_{\rm RLOF}. \quad (5)$$

This corresponds to the highest accretion rate that could potentially occur in a given system, but is most likely not

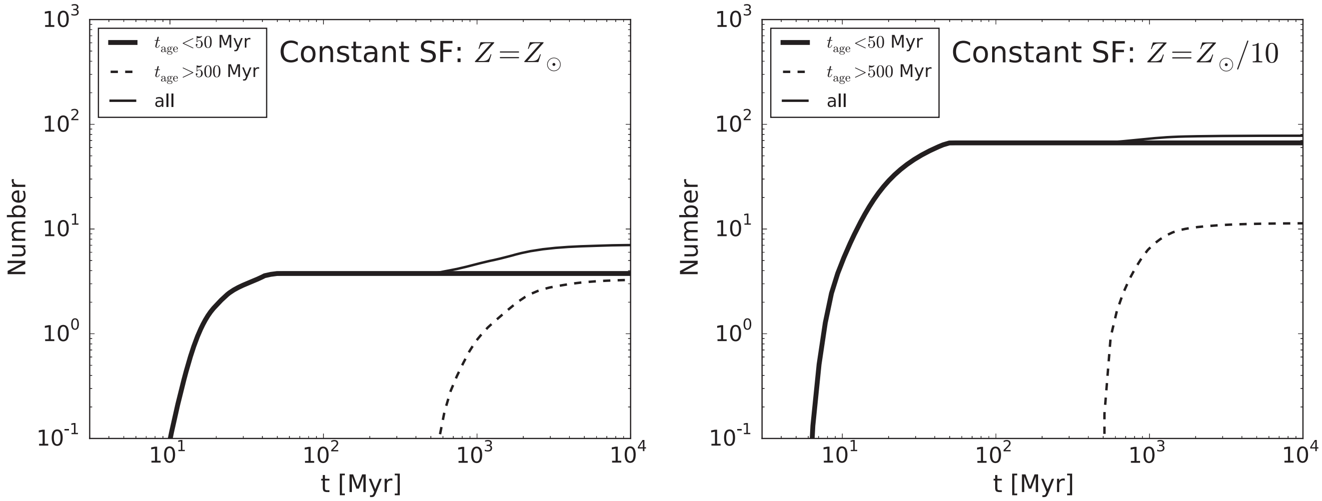

Figure 5. Evolution of the relative abundance of young ($t_{age} < 50$ Myr; mainly routes $\mathcal{R}_{BH,MS}$ and $\mathcal{R}_{NS,MS}$) and old ($t_{age} > 500$ Myr; mainly routes $\mathcal{R}_{NS,HG}$ and $\mathcal{R}_{NS,RG}$) ULXs through time for constant star-formation rate and two metallicities: $Z = Z_\odot$ (left) and $Z = Z_\odot/10$ (right).

realistic for high $\dot{M}_{RLOF}$. Therefore, this model should be considered as a rough upper limit for accretion.

The X-ray luminosity is calculated as

$$L_X = \frac{\epsilon G\, M_{BH/NS}\, \dot{M}_{RLOF}}{R_{acc}} = \eta\, \dot{M}_{RLOF} c^2, \tag{6}$$

where ϵ is a conversion efficiency of gravitational energy into radiation equal 1.0 for an NS (surface accretion) and 0.5 for a BH (disk accretion), $M_{BH/NS}$ is the mass of the accretor, R_{acc} is the radius of an NS (assumed to be 10 km) or a BH (3 Schwarzschild radii, non-rotating BH), and η is the radiative efficiency of a standard thin disk equal ~0.2 for an NS and 1/12 for a BH (e.g., Shakura & Sunyaev 1973).

A.2. Models of the Beaming

In addition to the beaming model described in Section 2.2 to which we will refer to as BK, we investigated also the following models:

A.2.1. No Beaming (BN)

For this model, we assumed isotropic emission, therefore,

$$b = 1 \tag{7}$$

for all systems and all MT rates.

A.2.2. Constant Beaming, no Saturation (B01)

We start with the simplest model of constant beaming, and we apply it to all sources. We consider only one case of $b = 0.1$ ($\theta \approx 52°$) to compare it with more realistic prescriptions described below. Such a constant beaming will lower the total luminosity, which is required for a source to be observed as a ULX to $b \times 10^{39}$ erg s^{-1}. This will generally increase the number of predicted ULX sources. On the other hand, $P_{obs,b}$ will be lower for all systems, which will decrease this number. These two processes may make the predicted number of ULXs lower or higher in comparison to models without beaming.

A.2.3. Sądowski's Model with Saturation (BS)

This beaming prescription is based mainly on the results of theoretical and numerical analyses presented in Lasota et al. (2016) and based on the results of KORAL (Sądowski et al. 2014) GRRMHD simulations. They showed that super-Eddington disks never become geometrically thick, because the thickness of the slim disk does not depend on the MT rate. Even for very high $\dot{m}$ the ratio of photosphere height (H) to radius (R) is $H/R \lesssim 1.6$. We fitted a phenomenological model to approximate the relation between H/R and $\dot{m}$ found by Lasota et al. (2016; Figure 4), and we obtained

$$\frac{H}{R} = \frac{1.6}{1 + \frac{4}{\dot{m}}} \tag{8}$$

for non-rotating BH accretion with non-saturated magnetic field. This relation corresponds to $R = 30\, R_G$, but H/R should not be significantly larger for other radii. The equation shows a moderate photosphere height also for sub-Eddington MT rates. We used the same prescription for NS accretors.

The H/R is related to the opening angle θ as

$$\left(\frac{H}{R}\right)^{-1} = \tan\frac{\theta}{2}, \tag{9}$$

which allows us to derive the beaming factor as

$$b = 1 - \cos\frac{\theta}{2}, \tag{10}$$

and the apparent isotropic luminosity is calculated as in Equation (2).

The beaming becomes nearly constant for $\dot{m} \gtrsim 100$, which gives the minimum opening angle $\theta_{min} \approx 64°$ ($b \approx 0.15$). The prescription works for the entire range of $\dot{m}$ and shows a small collimation also for nearly Eddington MT ($\dot{m} < 1$). However, below $\dot{m} \approx 0.12$ the beaming factor is always greater than $b > 0.95 (\theta > 170°)$.

A.2.4. Additional Characteristics of the Simulated Populations of ULXs

Table 5 contains the dependence of #ULX on $L_{X,min}$. The distributions of the general population's parameters are in Tables 6–10. The evolution of the #ULX through population age are in Figures 6 and 7. Tables 11–15 contain the distributions of companions.

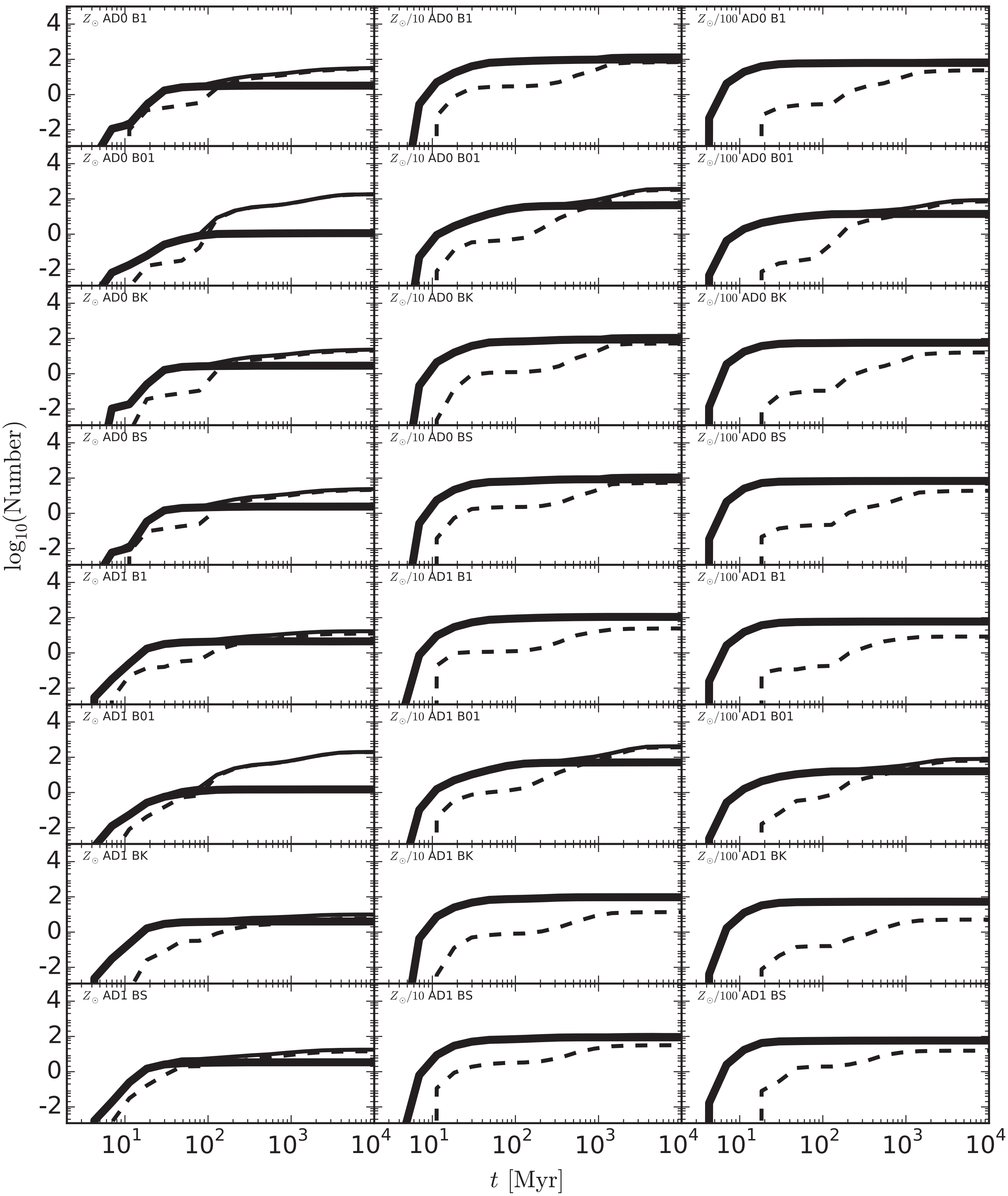

Figure 6. Relation between the number of ULXs and the age of the population for constant SFR of 6.0 $M_\odot$ yr^{-1} (total stellar mass equal Milky Way Equivalent Galaxy). The thick line corresponds to BHULXs, dashed to NSULXs, and solid to all ULXs. $Z_\odot$ depicts the solar metallicity, AD0/1 are the accretion models (Appendix A.1 and Section 2.1) and BN, B01, BK, and BS stand for beaming models (Appendix A.2 and Section 2.2).

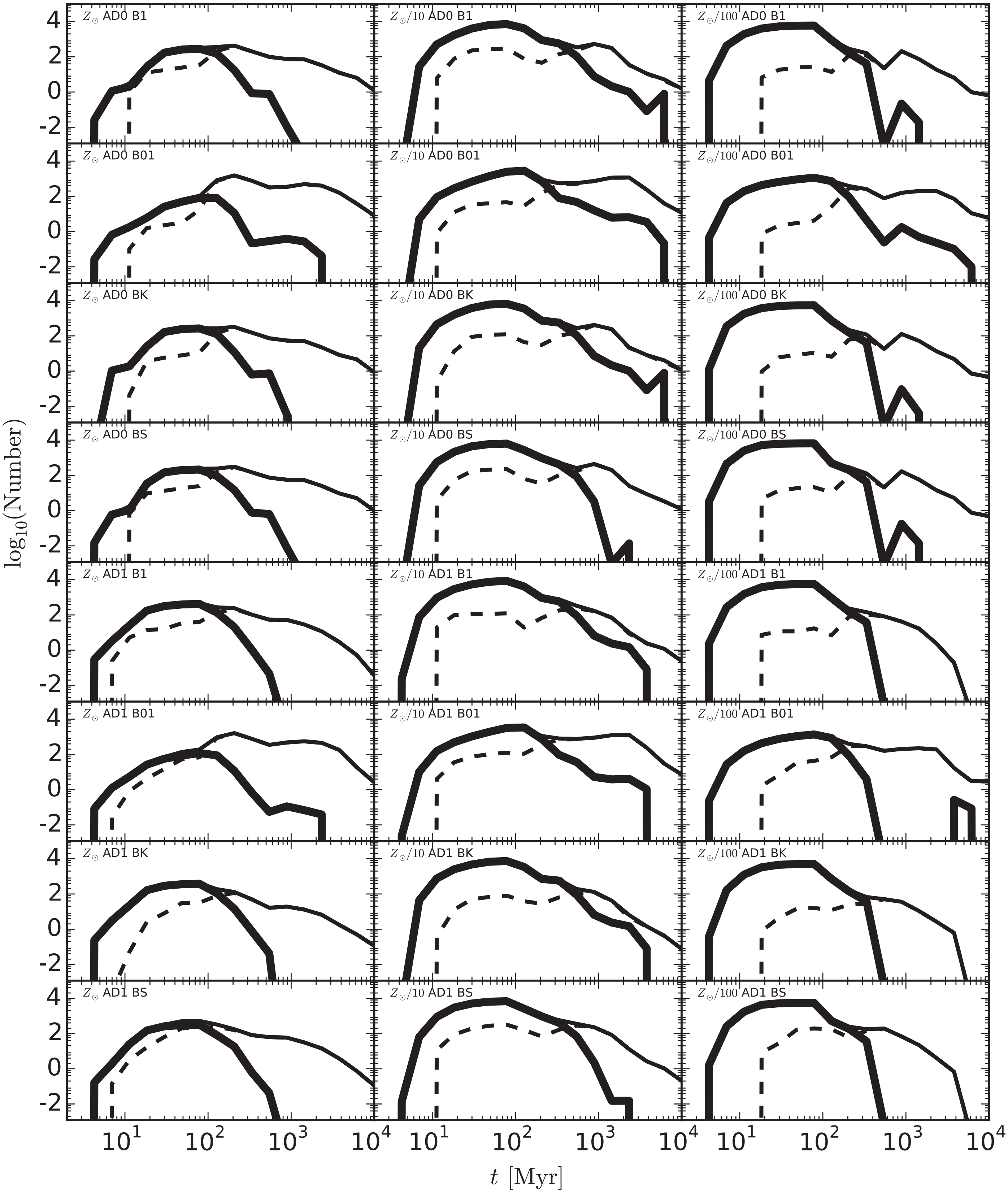

Figure 7. Same as in Figure 6, but for burst star formation with a duration of 100 Myr and SFR of 600 $M_\odot$ yr^{-1}.

Table 11
Companions (Constant SFR)

Model	MS	HG	RG	CHeB	HeMS	HeWD	HybWD	MS	HG	RG	HeMS	HeHG	HeGB	HeWD	COWD	HybWD
									$Z_{\odot}$							
AD0 BN	0.82	0.18	0.01					0.03	0.05	0.05	0.01	0.08		0.32	0.09	0.37
AD0 B01	0.91	0.07	0.02					0.02	0.02	0.01	0.16			0.38	0.10	0.32
AD0 BK	0.91	0.09						0.01	0.04	0.04	0.01	0.08		0.34	0.10	0.39
AD0 BS	0.92	0.08						0.01	0.06	0.03	0.03	0.09		0.33	0.09	0.35
AD1 BN	0.85	0.15						0.04	0.10	0.02	0.02	0.09	0.01	0.22	0.08	0.42
AD1 B01	0.94	0.05						0.05	0.04	0.01	0.15	0.01		0.33	0.10	0.32
AD1 BK	0.94	0.06						0.13	0.10	0.08	0.04	0.04		0.17	0.07	0.37
AD1 BS	0.94	0.06						0.09	0.16	0.05	0.02	0.08		0.23	0.08	0.30
									$Z_{\odot}/10$							
AD0 BN	0.68	0.30		0.01				0.06	0.47	0.02		0.01		0.21	0.07	0.17
AD0 B01	0.87	0.10						0.02	0.03		0.03			0.47	0.15	0.29
AD0 BK	0.74	0.24	0.01	0.01				0.03	0.51	0.01				0.21	0.07	0.16
AD0 BS	0.79	0.20	0.01	0.01				0.03	0.49	0.01		0.01		0.22	0.07	0.17
AD1 BN	0.69	0.28		0.02				0.10	0.39	0.02		0.02		0.19	0.08	0.21
AD1 B01	0.91	0.08						0.06	0.04	0.01	0.03			0.42	0.15	0.30
AD1 BK	0.76	0.21	0.01	0.01				0.11	0.54	0.05				0.13	0.05	0.13
AD1 BS	0.81	0.17	0.01	0.01				0.08	0.52	0.03		0.01		0.16	0.06	0.15
									$Z_{\odot}/100$							
AD0 BN	0.77	0.09		0.13	0.01			0.02	0.48	0.04		0.06		0.25	0.01	0.13
AD0 B01	0.89	0.04		0.06				0.03	0.03	0.03	0.07			0.56	0.03	0.25
AD0 BK	0.83	0.05		0.12				0.01	0.48	0.04		0.04		0.27	0.01	0.14
AD0 BS	0.87	0.05		0.08				0.02	0.29	0.12		0.04		0.35	0.02	0.18
AD1 BN	0.76	0.10		0.13	0.01			0.04	0.45	0.05		0.13		0.14	0.01	0.18
AD1 B01	0.91	0.04		0.05				0.13	0.05	0.06	0.07			0.33	0.03	0.31
AD1 BK	0.84	0.06		0.10				0.12	0.47	0.20		0.03		0.07	0.01	0.10
AD1 BS	0.89	0.05		0.06				0.10	0.36	0.27		0.03		0.11	0.01	0.12

Note. Companions (donors) in ULXs formed in models with constant SFR. Fractions for different companion types are provided separately for BHULXs and NSULXs. The age of the population is 10 Gyr.

Table 12
Companions (Burst SFR 100 Myr Ago)

Model	MS	HG	RG	CHeB	HeMS	HeWD	HybWD	MS	HG	RG	HeMS	HeHG	HeGB	HeWD	COWD	HybWD
									$Z_{\odot}$							
AD0 BN	0.89	0.11						0.42			0.02	0.49	0.01			0.06
AD0 B01	0.96	0.03						0.01			0.98	0.01				
AD0 BK	0.97	0.03						0.29			0.04	0.57				0.10
AD0 BS	0.97	0.03						0.07			0.67	0.22				0.03
AD1 BN	0.90	0.10						0.28				0.59	0.12			
AD1 B01	0.97	0.03						0.14			0.85	0.01				
AD1 BK	0.98	0.02						0.89				0.10				
AD1 BS	0.97	0.03						0.73			0.11	0.15	0.01			
									$Z_{\odot}/10$							
AD0 BN	0.86	0.11		0.02	0.01			0.98			0.01	0.01				
AD0 B01	0.97	0.03						0.97			0.02	0.01				
AD0 BK	0.94	0.04		0.01				0.98			0.02	0.01				
AD0 BS	0.95	0.03		0.01				0.96			0.03	0.01				
AD1 BN	0.85	0.12		0.03	0.01			0.94			0.01	0.04	0.02			
AD1 B01	0.97	0.03		0.01				0.99			0.01					
AD1 BK	0.94	0.03		0.02				1.00								
AD1 BS	0.95	0.04		0.01				0.99								
									$Z_{\odot}/100$							
AD0 BN	0.81	0.05		0.13	0.01			0.97				0.02				
AD0 B01	0.91	0.02		0.06				0.88			0.10	0.01				
AD0 BK	0.86	0.01		0.12				0.98			0.01	0.01				0.01
AD0 BS	0.90	0.02		0.08				0.85			0.12	0.01				0.01
AD1 BN	0.79	0.06		0.14	0.01			0.60				0.27	0.13			
AD1 B01	0.92	0.02		0.05				0.98			0.01	0.01				
AD1 BK	0.87	0.02		0.11				1.00								
AD1 BS	0.92	0.02		0.06				0.98				0.02				

Note. Companions (donors) in ULXs formed in models with burst SF. Start of the burst was 100 Myr ago and its duration was 100 Myr.

Table 13
Companions (Burst SFR 1 Gyr Ago)

Model	MS	HG	RG	CHeB	HeMS	HeWD	HybWD	MS	HG	RG	HeMS	HeHG	HeGB	HeWD	COWD	HybWD
									$Z_{\odot}$							
AD0 BN		1.00						0.02	0.07					0.49	0.09	0.33
AD0 B01	0.28	0.43	0.29					0.07	0.03					0.12	0.03	0.74
AD0 BK		1.00						0.01	0.07					0.49	0.09	0.33
AD0 BS		1.00						0.02	0.12					0.46	0.08	0.31
AD1 BN			1.00					0.01	0.31		0.01			0.35	0.07	0.25
AD1 B01	0.51	0.01	0.47		0.01			0.15	0.17	0.02				0.09	0.02	0.54
AD1 BK			1.00					0.03	0.41		0.01			0.29	0.06	0.20
AD1 BS			1.00					0.04	0.47					0.26	0.05	0.17
									$Z_{\odot}/10$							
AD0 BN	0.40	0.37	0.18					0.01	0.74					0.17	0.03	0.05
AD0 B01	0.32	0.44	0.23					0.03	0.08					0.32	0.05	0.51
AD0 BK	0.41	0.34	0.19						0.78					0.15	0.03	0.05
AD0 BS	0.40	0.37	0.18					0.01	0.58					0.28	0.05	0.08
AD1 BN	0.60	0.10	0.24					0.04	0.47					0.33	0.06	0.11
AD1 B01	0.64	0.22	0.13					0.08	0.11					0.28	0.05	0.47
AD1 BK	0.60	0.10	0.24					0.03	0.73	0.01				0.15	0.03	0.05
AD1 BS	0.58	0.12	0.25					0.02	0.63	0.01				0.23	0.04	0.07
									$Z_{\odot}/100$							
AD0 BN		0.87	0.03	0.10					0.79					0.17	0.01	0.03
AD0 B01	0.12	0.47	0.38				0.03	0.01	0.10	0.01				0.36	0.01	0.51
AD0 BK		1.00							0.79					0.17	0.01	0.03
AD0 BS		0.90	0.02	0.07					0.60					0.32	0.02	0.05
AD1 BN									0.46	0.02				0.43	0.03	0.07
AD1 B01								0.19	0.08	0.02				0.29	0.01	0.42
AD1 BK								0.12	0.57	0.10				0.17	0.01	0.03
AD1 BS								0.05	0.46	0.12				0.30	0.02	0.04

Note. Companions (donors) in ULXs formed in models with burst SF. Start of the burst was 1 Gyr ago and its duration was 100 Myr.

Table 14
Companions (Burst SFR 5 Gyr Ago)

Model	MS	HG	RG	CHeB	HeMS	HeWD	HybWD	MS	HG	RG	HeMS	HeHG	HeGB	HeWD	COWD	HybWD
									$Z_{\odot}$							
AD0 BN										0.37				0.63		
AD0 B01										0.01				0.75	0.24	
AD0 BK										0.32				0.68		
AD0 BS										0.19				0.81		
AD1 BN										0.31				0.69		
AD1 B01										0.02				0.63	0.35	
AD1 BK										0.78				0.22		
AD1 BS										0.61				0.39		
									$Z_{\odot}/10$							
AD0 BN										0.16				0.56	0.28	
AD0 B01								0.01		0.02				0.70	0.27	
AD0 BK										0.17				0.55	0.28	
AD0 BS										0.21				0.53	0.26	
AD1 BN										0.02				0.43	0.54	
AD1 B01								0.01		0.04				0.54	0.41	
AD1 BK										0.25				0.34	0.41	
AD1 BS										0.38				0.28	0.34	
									$Z_{\odot}/100$							
AD0 BN								0.10		0.25				0.66		
AD0 B01						1.00		0.02	0.03	0.17				0.77		
AD0 BK								0.04		0.30				0.66		
AD0 BS								0.02		0.60				0.38		
AD1 BN										1.00						
AD1 B01						0.17		0.09	0.10	0.68				0.08		
AD1 BK								0.38		0.62						
AD1 BS								0.03		0.97						

Note. Companions (donors) in ULXs formed in models with burst SF. Start of the burst was 5 Gyr ago and its duration was 100 Myr.

Table 15
Companions (Burst SFR 10 Gyr Ago)

Model	MS	HG	RG	CHeB	HeMS	HeWD	HybWD	MS	HG	RG	HeMS	HeHG	HeGB	HeWD	COWD	HybWD
$Z_{\odot}$																
AD0 BN										0.40				0.60		
AD0 B01										0.08				0.92		
AD0 BK										0.38				0.62		
AD0 BS										0.40				0.60		
AD1 BN										0.19				0.81		
AD1 B01										0.31				0.69		
AD1 BK										0.92				0.08		
AD1 BS										0.91				0.09		
$Z_{\odot}/10$																
AD0 BN														0.83	0.17	
AD0 B01										0.07				0.73	0.20	
AD0 BK														0.83	0.17	
AD0 BS														0.83	0.17	
AD1 BN														0.89	0.11	
AD1 B01										0.11				0.56	0.34	
AD1 BK														0.90	0.10	
AD1 BS														0.89	0.11	
$Z_{\odot}/100$																
AD0 BN														1.00		
AD0 B01								0.05	0.07	0.12				0.54		
AD0 BK														1.00		
AD0 BS														1.00		
AD1 BN										1.00						
AD1 B01								0.11	0.13	0.27				0.01		
AD1 BK										1.00						
AD1 BS										1.00						

Note. Companions (donors) in ULXs formed in models with burst SF. Start of the burst was 10 Gyr ago and its duration was 100 Myr. A total absence of BHULXs may be observed.

References

Abt, H. A. 1983, ARA&A, 21, 343
Bachetti, M., Harrison, F. A., Walton, D. J., et al. 2014, Natur, 514, 202
Begelman, M. C. 2002, ApJL, 568, L97
Belczynski, K., Bulik, T., Fryer, C. L., et al. 2010, ApJ, 714, 1217
Belczynski, K., Holz, D. E., Bulik, T., & O'Shaughnessy, R. 2016, Natur, 534, 512
Belczynski, K., Kalogera, V., & Bulik, T. 2002, ApJ, 572, 407
Belczynski, K., Kalogera, V., Rasio, F. A., et al. 2008, ApJS, 174, 223
Coburn, W., Heindl, W. A., Gruber, D. E., et al. 2001, ApJ, 552, 738
de Mink, S. E., & Belczynski, K. 2015, ApJ, 814, 58
Dominik, M., Belczynski, K., Fryer, C., et al. 2012, ApJ, 759, 52
Duquennoy, A., & Mayor, M. 1991, A&A, 248, 485
Fabbiano, G., Zezas, A., & Murray, S. S. 2001, ApJ, 554, 1035
Fabrika, S. 2004, ASPRv, 12, 1
Feng, H., & Soria, R. 2011, NAR, 55, 166
Fragos, T., Linden, T., Kalogera, V., & Sklias, P. 2015, ApJL, 802, L5
Fürst, F., Walton, D. J., Harrison, F. A., et al. 2016, ApJL, 831, L14
Fürst, F., Walton, D. J., Stern, D., et al. 2017, ApJ, 834, 77
Gao, Y., Wang, Q. D., Appleton, P. N., & Lucas, R. A. 2003, ApJL, 596, L171
Gladstone, J. C., Copperwheat, C., Heinke, C. O., et al. 2013, ApJS, 206, 14
Grimm, H.-J., Gilfanov, M., & Sunyaev, R. 2003, MNRAS, 339, 793
Heida, M., Jonker, P. G., Torres, M. A. P., et al. 2014, MNRAS, 442, 1054
Heida, M., Jonker, P. G., Torres, M. A. P., et al. 2016, MNRAS, 459, 771
Irwin, J. A., Bregman, J. N., & Athey, A. E. 2004, ApJL, 601, L143
Israel, G. L., Belfiore, A., Stella, L., et al. 2017a, Sci, 355, 817
Israel, G. L., Papitto, A., Esposito, P., et al. 2017b, MNRAS, 466, L48
Jiang, Y.-F., Stone, J. M., & Davis, S. W. 2014, ApJ, 796, 106
King, A., & Lasota, J.-P. 2016, MNRAS, 458, L10
King, A., Lasota, J.-P., & Kluźniak, W. 2017, MNRAS, 468, L59
King, A. R. 2009, MNRAS, 393, L41
King, A. R., Davies, M. B., Ward, M. J., Fabbiano, G., & Elvis, M. 2001, ApJL, 552, L109
Kluźniak, W., & Lasota, J.-P. 2015, MNRAS, 448, L43
Körding, E., Falcke, H., & Markoff, S. 2002, A&A, 382, L13
Kroupa, P., & Weidner, C. 2003, ApJ, 598, 1076
Lasota, J.-P. 2016, ASSL, 440, 1
Lasota, J.-P., Vieira, R. S. S., Sadowski, A., Narayan, R., & Abramowicz, M. A. 2016, A&A, 587, A13
Licquia, T. C., & Newman, J. A. 2015, ApJ, 806, 96
Linden, T., Kalogera, V., Sepinsky, J. F., et al. 2010, ApJ, 725, 1984
Luangtip, W., Roberts, T. P., Mineo, S., et al. 2015, MNRAS, 446, 470
Mapelli, M., Colpi, M., & Zampieri, L. 2009, MNRAS, 395, L71
Mapelli, M., Ripamonti, E., Zampieri, L., Colpi, M., & Bressan, A. 2010, MNRAS, 408, 234
Mennekens, N., & Vanbeveren, D. 2014, A&A, 564, A134
Mineo, S., Gilfanov, M., & Sunyaev, R. 2012, MNRAS, 419, 2095
Motch, C., Pakull, M. W., Soria, R., Grisé, F., & Pietrzyński, G. 2014, Natur, 514, 198
Mushotzky, R. 2006, AdSpR, 38, 2793
Ohsuga, K., & Mineshige, S. 2011, ApJ, 736, 2
Ohsuga, K., Mori, M., Nakamoto, T., & Mineshige, S. 2005, ApJ, 628, 368
Pakull, M. W., & Mirioni, L. 2002, arXiv:astro-ph/0202488
Pavlovskii, K., Ivanova, N., Belczynski, K., & Van, K. X. 2017, MNRAS, 465, 2092
Pinto, C., Middleton, M. J., & Fabian, A. C. 2016, Natur, 533, 64
Pintore, F., Zampieri, L., Stella, L., et al. 2017, ApJ, 836, 113
Poutanen, J., Lipunova, G., Fabrika, S., Butkevich, A. G., & Abolmasov, P. 2007, MNRAS, 377, 1187
Prestwich, A. H., Tsantaki, M., Zezas, A., et al. 2013, ApJ, 769, 92
Roberts, T. P., Levan, A. J., & Goad, M. R. 2008, MNRAS, 387, 73
Sana, H., de Mink, S. E., de Koter, A., et al. 2012, Sci, 337, 444
Sądowski, A., & Narayan, R. 2015, MNRAS, 453, 3213
Sądowski, A., Narayan, R., McKinney, J. C., & Tchekhovskoy, A. 2014, MNRAS, 439, 503
Shakura, N. I., & Sunyaev, R. A. 1973, A&A, 24, 337
Shao, Y., & Li, X.-D. 2015, ApJ, 802, 131
Soria, R. 2007, in IAU Symp. 238, Black Holes from Stars to Galaxies—Across the Range of Masses, ed. V. Karas & G. Matt (Cambridge: Cambridge Univ. Press), 235
Soria, R., Cropper, M., Pakull, M., Mushotzky, R., & Wu, K. 2005, MNRAS, 356, 12
Swartz, D. A., Ghosh, K. K., Tennant, A. F., & Wu, K. 2004, ApJS, 154, 519
Swartz, D. A., Soria, R., Tennant, A. F., & Yukita, M. 2011, ApJ, 741, 49
Tsygankov, S. S., Doroshenko, V., Lutovinov, A. A., Mushtukov, A. A., & Poutanen, J. 2017, arXiv:1702.00966
Wang, S., Qiu, Y., Liu, J., & Bregman, J. N. 2016, ApJ, 829, 20
White, N. E., Nagase, F., & Parmar, A. N. 1995, in X-ray Binaries, ed. W. H. G. Lewin, J. van Paradijs, & E. P. J. van den Heuvel (Cambridge: Cambridge Univ. Press), 1
Wiktorowicz, G., Belczynski, K., & Maccarone, T. 2014, in arXiv:1312.5924
Wiktorowicz, G., Sobolewska, M., Sądowski, A., & Belczynski, K. 2015, ApJ, 810, 20
Xu, X.-J., & Li, X.-D. 2010, ApJ, 722, 1985
Zampieri, L., & Roberts, T. P. 2009, MNRAS, 400, 677